Group contribution methodology based on the statistical associating fluid theory for heteronuclear molecules formed from Mie segments

Vasileios Papaioannou, Thomas Lafitte, Carlos Avendaño, Claire S. Adjiman, George Jackson, Erich A. Müller, and Amparo Galindo

Citation: J. Chem. Phys. **140**, 054107 (2014); doi: 10.1063/1.4851455
View online: https://doi.org/10.1063/1.4851455
View Table of Contents: http://aip.scitation.org/toc/jcp/140/5
Published by the American Institute of Physics

Articles you may be interested in

Accurate statistical associating fluid theory for chain molecules formed from Mie segments
The Journal of Chemical Physics **139**, 154504 (2013); 10.1063/1.4819786

A group contribution method for associating chain molecules based on the statistical associating fluid theory (SAFT-γ)
The Journal of Chemical Physics **127**, 234903 (2007); 10.1063/1.2813894

Statistical associating fluid theory for chain molecules with attractive potentials of variable range
The Journal of Chemical Physics **106**, 4168 (1997); 10.1063/1.473101

Simultaneous estimation of phase behavior and second-derivative properties using the statistical associating fluid theory with variable range approach
The Journal of Chemical Physics **124**, 024509 (2006); 10.1063/1.2140276

Perturbation Theory and Equation of State for Fluids. II. A Successful Theory of Liquids
The Journal of Chemical Physics **47**, 4714 (1967); 10.1063/1.1701689

Equilibrium Thermodynamic Properties of the Mixture of Hard Spheres
The Journal of Chemical Physics **54**, 1523 (1971); 10.1063/1.1675048

PHYSICS TODAY
WHITEPAPERS

ADVANCED LIGHT CURE ADHESIVES

Take a closer look at what these environmentally friendly adhesive systems can do

READ NOW

PRESENTED BY
MASTERBOND
ADHESIVES | SEALANTS | COATINGS

Group contribution methodology based on the statistical associating fluid theory for heteronuclear molecules formed from Mie segments

Vasileios Papaioannou,[1] Thomas Lafitte,[1] Carlos Avendaño,[1,2] Claire S. Adjiman,[1] George Jackson,[1] Erich A. Müller,[1] and Amparo Galindo[1,a)]

[1]*Department of Chemical Engineering, Centre for Process Systems Engineering, Imperial College London, South Kensington Campus, London SW7 2AZ, United Kingdom*

[2]*School of Chemical Engineering and Analytical Sciences, University of Manchester, Sackville Street, Manchester M13 9PL, United Kingdom*

(Received 27 September 2013; accepted 3 December 2013; published online 4 February 2014)

A generalization of the recent version of the statistical associating fluid theory for variable range Mie potentials [Lafitte *et al.*, J. Chem. Phys. **139**, 154504 (2013)] is formulated within the framework of a group contribution approach (SAFT-γ Mie). Molecules are represented as comprising distinct functional (chemical) groups based on a fused heteronuclear molecular model, where the interactions between segments are described with the Mie (generalized Lennard-Jonesium) potential of variable attractive and repulsive range. A key feature of the new theory is the accurate description of the monomeric group-group interactions by application of a high-temperature perturbation expansion up to third order. The capabilities of the SAFT-γ Mie approach are exemplified by studying the thermodynamic properties of two chemical families, the *n*-alkanes and the *n*-alkyl esters, by developing parameters for the methyl, methylene, and carboxylate functional groups (CH_3, CH_2, and COO). The approach is shown to describe accurately the fluid-phase behavior of the compounds considered with absolute average deviations of 1.20% and 0.42% for the vapor pressure and saturated liquid density, respectively, which represents a clear improvement over other existing SAFT-based group contribution approaches. The use of Mie potentials to describe the group-group interaction is shown to allow accurate simultaneous descriptions of the fluid-phase behavior and second-order thermodynamic derivative properties of the pure fluids based on a single set of group parameters. Furthermore, the application of the perturbation expansion to third order for the description of the reference monomeric fluid improves the predictions of the theory for the fluid-phase behavior of pure components in the near-critical region. The predictive capabilities of the approach stem from its formulation within a group-contribution formalism: predictions of the fluid-phase behavior and thermodynamic derivative properties of compounds not included in the development of group parameters are demonstrated. The performance of the theory is also critically assessed with predictions of the fluid-phase behavior (vapor-liquid and liquid-liquid equilibria) and excess thermodynamic properties of a variety of binary mixtures, including polymer solutions, where very good agreement with the experimental data is seen, without the need for adjustable mixture parameters. © *2014 Author(s). All article content, except where otherwise noted, is licensed under a Creative Commons Attribution 3.0 Unported License.* [http://dx.doi.org/10.1063/1.4851455]

I. INTRODUCTION

Thermodynamic tools are being continually developed and improved in order to meet the need for accurate property prediction in many sectors of the chemical industries. Predictive approaches have come to play an important role in the design of processes and the accuracy of the description of the thermodynamic properties can significantly affect process-design decisions.[1,2] Despite the wide variety of methods that are available, industrial requirements in property prediction highlight the need for approaches that can be applied in an ever-expanding range of applications, including, among others, polymer processing, biotechnology, and solvent screening.[3] Advances in thermodynamic modeling have led to novel applications, such as the integrated design of solvents and processes, where molecular characteristics of solvents are determined as part of the optimization of the process.[4–7] An important aspect in the development of thermodynamic methodologies is a predictive capability, which is commonly perceived as the ability to provide predictions of phase behavior and other bulk properties without the need for experimental data for the determination of molecular model parameters.

An important class of thermodynamic methodologies with high predictive power include group contribution (GC) approaches. GC methods are developed based on the assumption that the properties of a given compound can be determined as appropriate functions of the chemically distinct functional groups that the compound comprises. The contribution of each functional group to the molecular properties

a)Author to whom correspondence should be addressed. Electronic mail: a.galindo@imperial.ac.uk

 © Author(s) 2014

is assumed to be independent of the molecular structure that the group appears in. Such approaches have a long history of research and application; the first developments focused on the prediction of pure-component properties, such as the GC methods of Lydersen,[8] Joback and Reid,[9] and the subsequent work of Gani and co-workers,[10,11] to name but a few. Furthermore, GC approaches have found extensive application to the study of the thermodynamic properties of binary and multicomponent mixtures, often with an emphasis on fluid-phase behavior, initially within the framework of activity coefficient methods. An example of this type of methodology is the well-established universal quasi-chemical functional group activity coefficient (UNIFAC) formalism.[12] The UNIFAC approach and its subsequent modifications[13] are widely considered to be the state-of-the-art predictive methodologies for industrial applications due to their accuracy in predicting the phase behavior of a wide range of mixtures and the availability of extensive parameter tables. Alongside UNIFAC other predictive activity coefficient approaches have been developed, a prominent example of which is the computational-chemistry based conductor-like screening model for real solvents (COSMO-RS).[14] Such methods are however subject to a number of limitations: in these approaches one resorts to a treatment of the liquid phase only, neglecting pressure effects and only the subset of thermodynamic properties that can be determined from activity coefficients are obtained. With the aim of overcoming these limitations, GC methods have been coupled with equations of state (EoSs); prominent examples include the PSRK EoS,[15] the GC[16] and GCA[17] EoSs, and more recently the VTPR EoS.[18–20] Equations of state have the advantage of treating the vapor and liquid phases on an equal footing, can account for pressure effects, and can be applied to the study of a wide range of thermodynamic properties. Of particular relevance to the work presented in our current paper are the applications of GC within the framework of the statistical associating fluid theory (SAFT).[21,22] These are reviewed briefly in the following discussion; for more details of the different applications of GC methods, the reader is directed to the reviews of Refs. 23 and 24.

Various versions of the SAFT EoS have been successfully applied to the study of the properties of thermodynamically challenging systems, such as polymeric, hydrogen-bonding, and reactive systems. Details of the underlying theory and the different applications of SAFT can be found in a number of comprehensive reviews.[25–28] Early work dedicated to developing SAFT-based GC approaches involved the application of the group contribution concept at the level of determining the molecular parameters that describe a compound. In these *homonuclear* approaches the molecular model employed was the traditional SAFT representation of molecular chains formed from identical bonded segments, with all segments described by the same set of parameters, so that the underlying theory remained unchanged. Lora *et al.*[29] were one of the first to combine a group contribution method with the original SAFT EoS,[21,22] determining the molecular parameters that describe several poly(acrylates) by examining compounds of lower molecular weight. Subsequently, Vijande *et al.*[30] developed a SAFT-based GC approach with an emphasis on the prediction of the properties of hydrofluoroethers. In the same spirit, Tamouza *et al.*[31,32] have developed GC methods based on SAFT approaches which employ both fixed and variable-range interaction potentials for the study of the chemical families of the *n*-alkanes, alkylbenzenes, olefins, and alcohols. The methodology was then extended to account explicitly for interactions due to polarity (based on the treatment of Gubbins and Twu[33]) for the study of light and heavy esters,[34] and has since been applied to a wide range of systems including polycyclic hydrocarbons,[35] ethers, aldehydes, ketones,[36] amines,[37] and long-chain multifunctional molecules including alkanediols and alkanolamines.[38] Alongside the aforementioned SAFT-based group contribution methods, other techniques have been developed where molecular properties are not calculated as functions of the occurrences of functional groups alone, but also account for the positioning of the groups in the molecule by defining superstructures. In the context of GC methods this invariably involves a consideration of second-order groups (as in the work of Constantinou and Gani[10]). The aim of such an approach is to account for proximity effects (i.e., how the presence of a functional group influences the physicochemical properties of a neighboring group) and to distinguish the representation of isomers.[39–41]

As has been mentioned earlier, *homonuclear* SAFT-based GC can be used successfully to describe the thermodynamic properties of a wide range of systems. Nevertheless, the predictive capabilities of these methodologies are typically limited to the prediction of the properties of pure compounds as no information on the nature of the unlike interactions between groups and/or molecules can be extracted from the pure-component data that are used in the characterization of the functional groups. The determination of the unlike interaction parameters, which can also be calculated in a GC fashion as described by Le Thi *et al.*,[42] typically relies on the use of experimental data for mixtures. Methods based on London's theory can also be used to predict the values of the unlike interaction parameters from the physicochemical properties of the molecules within the SAFT formalism:[43] this type of approach has been applied to mixtures of CO_2, methane, and ethane with *n*-alkanes,[44,45] methanol with *n*-alkanes,[46] and aqueous solutions of alkanes, aromatic hydrocarbons, and alcohols.[36]

Group contribution approaches have also been developed within the framework of SAFT incorporating *heteronuclear* molecular models (and the corresponding theory). In *heteronuclear* approaches molecules are represented as chains of segments that are not necessarily identical. Within the Wertheim TPT1 methodology[47–53] it is possible to develop formally, on the premise of a detailed heteronuclear molecular model, an equation of state maintaining a link between the nature of the different segments making up the molecules and the corresponding parameters. The first such studies of bonded heteronuclear models formed from hard-sphere segments included heteronuclear dimer,[54] linear triatomic,[55] and arbitrary polyatomic molecules.[56,57] Within the context of a SAFT treatment, several variants have been reformulated based on a heteronuclear tangent molecular model. Examples include the work of Banaszak *et al.*,[58,59] Adidharma and Radosz,[60,61] McCabe *et al.*[62] and Peng *et al.*[63] who

implement a square-well (SW) potential to describe the group-group interactions, the work of Blas and Vega[64] based on molecules formed from Lennard-Jones (LJ) segments, and the work of Gross *et al.*[65] As well as describing molecules with heteronuclear models, it is apparent that a model with *fused* (as opposed to tangent) segments is needed to provide accurate thermodynamic properties of real fluids.[66,67] Fused models are treated within the SAFT-γ GC approach by representing the heteronuclear molecules as fused SW segments of different type with a shape factor to characterize the degree of overlap between the different groups. The method was shown to describe accurately the fluid-phase behavior of a wide range of pure components including the chemical families of *n*-alkanes, branched alkanes, alkylbenzenes, olefins, carboxylic acids, alcohols, ketones, and amines,[66,67] and was used to study aqueous solutions of alkanes and alcohols,[68] and systems of ionic liquids.[69] Peng *et al.*[70] have presented a closely related heteronuclear generalization of the SAFT-VR EoS based on the use of SW potentials. As discussed in a recent review,[28] the two theories, which were developed independently, are essentially identical, the only distinguishing feature being the treatment of the contribution due to the formation of chain-like molecules from distinct functional groups. Within the SAFT-γ EoS the contribution to the free energy due to the formation of the heteronuclear chain molecules is calculated based on a molecular average of the contact value of the radial distribution function; in the case of the GC-SAFT-VR EoS of Peng *et al.*[70] the contact values of the different monomeric segments are appropriately summed, with the aim to retain the connectivity of the distinct groups that form the molecule. As shown in the Appendix both approaches provide an essentially equivalent description of the thermodynamic properties of heteronuclear diatomic and triatomic molecules. We should also mention that a similar treatment to that of Peng *et al.*[70] has been followed in the recent work of Paduszyński and Domańska.[71] A key advantage of heteronuclear molecular approaches is that they can be used to predict the thermodynamic properties of mixtures based on unlike interaction parameters obtained from pure-component data alone.

In the context of group contribution approaches based on heteronuclear molecular models only potentials comprising hard-repulsive cores (e.g., the hard-sphere or square-well potentials) or of fixed form (e.g., the Lennard-Jones potential) have been considered thus far to describe the interactions between the molecular segments. Both the SW and the LJ form of interaction provide a successful representation of the fluid-phase equilibria for a wide variety of systems, but are known to have limitations. Potentials with infinitely repulsive cores are limited in the range of properties that can be described accurately (e.g., the inability to provide a simultaneous description of the fluid-phase behavior and thermodynamic derivative properties), due to the simplified representation of intermolecular forces.[72,73] On the other hand, potentials of fixed form are limited in terms of the types of compound that can be represented accurately. As an example, the LJ potential cannot be applied to describe the intermolecular interactions of perfluorocarbons which are known to be characterized by much steeper repulsive interactions than can be represented with the LJ form.[74] The development of a SAFT-based group contribution approach that incorporates the versatile Mie intermolecular potential of variable attractive and repulsive range is a key objective of our current work. We show that the resulting SAFT-γ Mie methodology constitutes a thermodynamic approach with a high predictive capability that can be applied to a wide variety of systems of different chemical nature providing an accurate description of thermodynamic properties, ranging from fluid-phase behavior to second-order derivative properties, such as the speed of sound, heat capacity, or isothermal compressibility.

Over the past decade there has been increased interest in the performance of EoSs in the description of second-order derivative properties. These derivative properties are of interest from a practical perspective (e.g., the use of the Joule-Thomson inversion curve in the Linde technique as a standard industrial process), and a precise description of such properties, for which the performance of traditional cubic EoSs has been shown to be relatively poor,[75–78] is highly challenging from a theoretical perspective.[75] An accurate representation of derivative properties is a stringent test even with a more sophisticated thermodynamic treatment such as SAFT. One of the first detailed studies of the performance of SAFT-type methods in the description of such properties was carried out by Colina *et al.*[79] These authors examined the Joule-Thomson inversion curve obtained with the LJ-based soft-SAFT EoS[64,80] and found that although good agreement could be achieved, the description was very sensitive to the values of the molecular parameters. In a subsequent study different versions of the SAFT EoS were compared, and deviations of up to 20% from the experimental values of the derivative properties were found.[81] Llovell *et al.*[82] have also presented a detailed analysis on the performance of the soft-SAFT EoS for the derivative properties of pure components and mixtures[83] concluding that the accuracy of the description can range from 1% to 20% depending on the compound and the property of interest, with the highest deviations typically obtained for the speed of sound of long-chain *n*-alkanes. In other work on smaller molecules where SW or LJ forms of the potential are implemented, the reported errors for the description of the derivative properties is found to be within 10%.[84] A number of studies have been carried out with the aim of improving the description of the derivative properties.[76,77,85–87] However, the simultaneous representation of fluid-phase behavior and derivative properties is found to come at a cost: Maghari *et al.*[86,87] have employed an empirical temperature dependence of the dispersion energy by means of compound-specific constants, while Kontogeorgis and co-workers[77] re-correlated the universal constants of the PC-SAFT EoS to include derivative property data.

Derivative properties have also been extensively studied with renormalization-group crossover approaches as their singular behavior at the critical point makes them especially interesting. Examples of such studies that relate to the general SAFT framework include the work of Llovell *et al.*,[88] Dias *et al.*,[89] Vilaseca *et al.*,[90] and Forte *et al.*[91] Other crossover methods have also been applied to the study of derivative properties, such as the crossover-cubic[92] and the crossover-lattice EoSs.[93]

An aim our current work is to demonstrate the impact of the intermolecular potential model that is employed within a SAFT GC treatment on the accuracy that can be achieved in the simultaneous description of the fluid-phase behavior and second-order derivative thermodynamic properties. It is important to note that SAFT approaches based on segment-segment interactions treated with Mie potentials of variable attractive and repulsive ranges are recognized to provide such a capability.[72,94]

An improved version of the SAFT-VR Mie EoS has been recently developed,[73] where the various approximations inherent in the underlying theory of the EoS presented in 2006[72,95] are revisited and the perturbation expansion (in the description of the free energy due to monomeric interactions) are taken to third order to incorporate the effect of higher-order contributions. The SAFT-VR Mie approach has been shown to be very accurate for the simultaneous description of the fluid-phase behavior and thermodynamic derivative properties of pure substances and mixtures. In view of its success in describing the thermodynamic properties of real systems, we now reformulate SAFT-VR Mie as a group contribution approach based on a heteronuclear model of fused segments interacting via Mie potentials of variable repulsive and attractive range: SAFT-γ Mie. The goal is to develop a predictive group-contribution capability that provides accurate thermodynamic properties, including both fluid-phase behavior and second-order derivatives of the free energy, such as the heat capacity, compressibility, or speed of sound.

The remainder of the paper is organized as follows: A brief discussion on the underlying molecular model and the intermolecular potential is first presented in Sec. II, followed by a detailed description of the SAFT-γ Mie group contribution approach (Sec. III) and the procedure adopted for the estimation of group parameters (Sec. IV). The parameters for the functional groups of two chemical families (*n*-alkanes and *n*-alkyl esters) are presented in Sec. V A and the performance of the theory in describing the fluid-phase behavior of pure compounds is thoroughly assessed. The predictive capabilities of the approach in the prediction of second-order thermodynamic derivatives of pure components and the fluid-phase behavior and excess properties of binary mixtures are demonstrated in Sec. V B.

II. MOLECULAR MODEL AND INTERMOLECULAR POTENTIAL

As with other group contribution approaches the determination of molecular properties with the SAFT-γ Mie EoS is achieved by subdividing the molecules into distinct functional groups chosen to represent their various chemical moieties, with appropriate summations over the contributions of each of the functional groups. A fused heteronuclear model is employed, where the molecules are constructed from distinct monomeric segments which in our case are taken to interact through Mie potentials of variable attractive and repulsive range. An example of the fused heteronuclear molecular model used to represent *n*-hexane is shown in Figure 1, where the CH_3 and CH_2 functional groups that characterize *n*-hexane are denoted. In line with physical expectations a fused

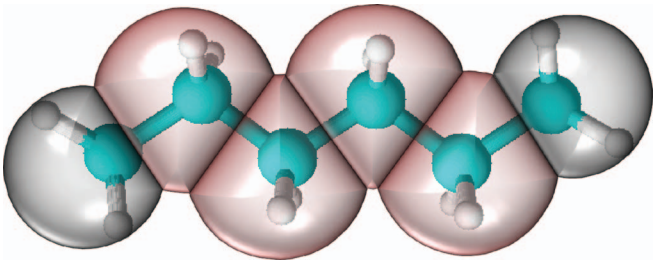

FIG. 1. Representation of a fused heteronuclear molecular model employed within the SAFT-γ Mie approach. The example depicted is for *n*-hexane, comprising two instances of the methyl CH_3 group (highlighted in gray), and four instances of the methylene CH_2 group (highlighted in red).

heteronuclear united-atom representation has been shown to be more appropriate than tangential heteronuclear models in the description of the fluid-phase equilibria of real compounds within a SAFT-γ treatment.[66] A potential of the Mie form has been used for homonuclear models within the SAFT-VR framework by Davies *et al.*,[96] as well as in the original development of the SAFT-VR Mie EoS.[72,95] The main difference between these two approaches is in the treatment of the radial distribution function (RDF) of the Mie fluid, which in the approach of Davies *et al.*[96] is approximated as the RDF of the Sutherland-6 potential. However, it is known that the accuracy of the representation of the RDF of the monomer reference system is of great importance in the development of EoSs based on the first-order thermodynamic perturbation theory (TPT1) of Wertheim.[47–50] In the latest incarnation of the SAFT-VR Mie EoS[73] an accurate second-order expansion of the RDF is developed; we use this latter form of the RDF in our current work.

The Mie intermolecular potential[97] is a generalized Lennard-Jonesium potential,[98–102] where the repulsive and attractive exponents which characterize the hardness/softness and the range of the interaction are allowed to vary freely. The form of the pair interaction energy between two segments k and l as a function of the intersegment distance r_{kl} is given by

$$\Phi_{kl}^{\mathrm{Mie}}(r_{kl}) = \mathcal{C}_{kl}\epsilon_{kl}\left[\left(\frac{\sigma_{kl}}{r_{kl}}\right)^{\lambda_{kl}^{\mathrm{r}}} - \left(\frac{\sigma_{kl}}{r_{kl}}\right)^{\lambda_{kl}^{\mathrm{a}}}\right], \qquad (1)$$

where σ_{kl} is the segment diameter, ϵ_{kl} is the depth of the potential well, and $\lambda_{kl}^{\mathrm{r}}$ and $\lambda_{kl}^{\mathrm{a}}$ are the repulsive and attractive exponents of the intersegment interactions, respectively. The prefactor $\mathcal{C}_{kl}$ is a function of these exponents and ensures that the minimum of the interaction is $-\epsilon_{kl}$:

$$\mathcal{C}_{kl} = \frac{\lambda_{kl}^{\mathrm{r}}}{\lambda_{kl}^{\mathrm{r}} - \lambda_{kl}^{\mathrm{a}}}\left(\frac{\lambda_{kl}^{\mathrm{r}}}{\lambda_{kl}^{\mathrm{a}}}\right)^{\frac{\lambda_{kl}^{\mathrm{a}}}{\lambda_{kl}^{\mathrm{r}} - \lambda_{kl}^{\mathrm{a}}}}. \qquad (2)$$

In common with other SAFT approaches, additional short-range association sites can be placed on the segments to mimic the association interactions (hydrogen bonding and other short-range interactions) present in some polar compounds. More specifically the association interactions are modeled by means of square-well sites, so that the interaction between a site of type a placed on a segment of type k

and a site of type b placed on a segment of type l is given by

$$\Phi^{\mathrm{HB}}_{kl,ab}(r_{kl,ab}) = \begin{cases} -\epsilon^{\mathrm{HB}}_{kl,ab} & \text{if } r_{kl,ab} \le r^{\mathrm{c}}_{kl,ab}, \\ 0 & \text{if } r_{kl,ab} > r^{\mathrm{c}}_{kl,ab}, \end{cases} \tag{3}$$

where $r_{kl,ab}$ is the center-center distance between sites a and b, $-\epsilon^{\mathrm{HB}}_{kl,ab}$ is the association energy, and $r^{\mathrm{c}}_{kl,ab}$ the cut-off range of the interaction between sites a and b. Each site is positioned at a distance $r^{\mathrm{d}}_{kk,aa}$ from the center of the segment on which it is placed.

We should also note that within the SAFT-γ treatment a group may comprise several identical segments.[67] The number of identical segments forming a group k is labeled ν^*_k. To summarize, the parameters that fully describe a functional group k are the number ν^*_k of identical segments that the group comprises, the diameter σ_{kk} of the segments of the group, the energy of interaction ϵ_{kk} between the segments of the group, and the values $\lambda^{\mathrm{r}}_{kk}$ and $\lambda^{\mathrm{a}}_{kk}$ of the repulsive and attractive exponents, respectively, that determine the form of the interaction potential. The extent to which the segments of a given group k contribute to the overall molecular properties is characterized with a key parameter of the methodology: the shape factor S_k. The interactions between groups of different types k and l are specified through the corresponding unlike parameters σ_{kl}, ϵ_{kl}, $\lambda^{\mathrm{r}}_{kl}$, and $\lambda^{\mathrm{a}}_{kl}$. In the case of associating groups, the number $N_{\mathrm{ST},k}$ of different site types, the number of sites of a given type, e.g., $n_{k,a}$, $n_{k,b}$, …, $n_{k,N_{\mathrm{ST},k}}$, together with the position $r^{\mathrm{d}}_{kl,ab}$ of the site, and the energy $\epsilon^{\mathrm{HB}}_{kl,ab}$ and range $r^{\mathrm{c}}_{kl,ab}$ of the association between sites, of the same or different type, have to be determined.

III. SAFT-γ MIE

The total Helmholtz free energy A of a mixture of heteronuclear associating molecules formed from Mie segments is written in dimensionless form as the sum of four separate contributions,

$$\frac{A}{Nk_{\mathrm{B}}T} = \frac{A^{\mathrm{ideal}}}{Nk_{\mathrm{B}}T} + \frac{A^{\mathrm{mono.}}}{Nk_{\mathrm{B}}T} + \frac{A^{\mathrm{chain}}}{Nk_{\mathrm{B}}T} + \frac{A^{\mathrm{assoc.}}}{Nk_{\mathrm{B}}T}, \tag{4}$$

where A^{ideal} is the free energy of the ideal gas, $A^{\mathrm{mono.}}$ is the term accounting for interactions between monomeric Mie segments, A^{chain} is the contribution to the free energy for the formation of molecules from Mie segments, $A^{\mathrm{assoc.}}$ is the term accounting for the association interactions, N is the total number of molecules, k_{B} is the Boltzmann constant, and T is the absolute temperature. In Secs. III A–III E, the separate contributions to the free energy are described in detail.

A. Ideal term

The ideal contribution to the free energy of the mixture is given by[103]

$$\frac{A^{\mathrm{ideal}}}{Nk_{\mathrm{B}}T} = \left(\sum_{i=1}^{N_{\mathrm{C}}} x_i \ln\left(\rho_i \Lambda_i^3\right) \right) - 1, \tag{5}$$

where x_i is the mole fraction of component i in the mixture, $\rho_i = N_i/V$ is the number density of component i, N_i being the number of molecules of component i and V the volume of the system. The summation in Eq. (5) is over all of the components N_{C} present in the mixture (and $N = \sum_{i=1}^{N_{\mathrm{C}}} N_i$). The ideal free energy incorporates the effects of the translational, rotational, and vibrational contributions to the kinetic energy implicitly through the thermal de Broglie volume, Λ_i^3.

B. Monomer term

The monomer term $A^{\mathrm{mono.}}$ describes the contribution of segment-segment interactions, taken to be of the Mie form in our case, to the total Helmholtz free energy of the system. This contribution is obtained with a Barker and Henderson[104,105] perturbation expansion to third order. The intermolecular potential of Eq. (1) is first written as the sum of a reference repulsive contribution $\Phi_0(r_{kl})$, and a perturbation attractive contribution $\Phi_1(r_{kl})$:

$$\Phi^{\mathrm{Mie}}_{kl}(r_{kl}) = \Phi_0(r_{kl}) + \Phi_1(r_{kl}), \tag{6}$$

where

$$\Phi_0(r_{kl}) = \begin{cases} \Phi^{\mathrm{Mie}}_{kl}(r_{kl}) & \text{if } r_{kl} \le \sigma_{kl}, \\ 0 & \text{if } r_{kl} > \sigma_{kl}, \end{cases} \tag{7}$$

and

$$\Phi_1(r_{kl}) = \begin{cases} 0 & \text{if } r_{kl} < \sigma_{kl}, \\ \Phi^{\mathrm{Mie}}_{kl}(r_{kl}) & \text{if } r_{kl} \ge \sigma_{kl}\,. \end{cases} \tag{8}$$

Barker and Henderson[105] have shown that the free energy of the system can then be obtained as a perturbation expansion in the inverse temperature with respect to the properties of the reference system. In the case of soft-core potentials, such as the Mie potential, the reference system can be approximated as an equivalent system of hard spheres with an effective (temperature-dependent) diameter d_{kk}, since the properties of the reference system described by the potential in Eq. (7) are not generally known. The high-temperature perturbation expansion can then be expressed as

$$\frac{A^{\mathrm{mono.}}}{Nk_{\mathrm{B}}T} = \frac{A^{\mathrm{HS}}}{Nk_{\mathrm{B}}T} + \frac{A_1}{Nk_{\mathrm{B}}T} + \frac{A_2}{Nk_{\mathrm{B}}T} + \frac{A_3}{Nk_{\mathrm{B}}T}, \tag{9}$$

where A^{HS} is the free energy of the hard-sphere reference system of diameter d_{kk}. For a given group k, the effective hard-sphere diameter is obtained from[105]

$$d_{kk} = \int_0^{\sigma_{kk}} \left[1 - \exp\left\{ -\frac{\Phi^{\mathrm{Mie}}_{kk}(r_{kk})}{k_{\mathrm{B}}T} \right\} \right] \mathrm{d}r\,. \tag{10}$$

The integral of Eq. (10) is obtained by means of Gauss-Legendre quadrature, a technique previously employed by Paricaud[106] who showed that a 5-point Gauss-Legendre procedure is adequate for an accurate representation of the effective hard-sphere diameter d_{kk}.

The hard-sphere Helmholtz free energy of the mixture is given by[66]

$$\frac{A^{\mathrm{HS}}}{Nk_{\mathrm{B}}T} = \left(\sum_{i=1}^{N_{\mathrm{C}}} x_i \sum_{k=1}^{N_{\mathrm{G}}} \nu_{k,i} \nu^*_k S_k \right) a^{\mathrm{HS}}, \tag{11}$$

where N_{G} is the number of types of groups present, $\nu_{k,i}$ the number of occurrences of a group of type k on component i, and a^{HS} is the dimensionless contribution to the hard-sphere

free energy per segment, obtained using the expression of Boublík[107] and Mansoori *et al.*:[108]

$$a^{\mathrm{HS}} = \frac{6}{\pi\rho_{\mathrm{s}}}\left[\left(\frac{\zeta_2^3}{\zeta_3^2} - \zeta_0\right)\ln(1-\zeta_3) + 3\frac{\zeta_1\zeta_2}{1-\zeta_3} + \frac{\zeta_2^3}{\zeta_3(1-\zeta_3)^2}\right]. \quad (12)$$

In Eq. (12), ρ_{s} is the segment number density which is related to the molecular density ρ through

$$\rho_{\mathrm{s}} = \rho\left(\sum_{i=1}^{N_{\mathrm{C}}} x_i \sum_{k=1}^{N_{\mathrm{G}}} \nu_{k,i}\nu_k^* S_k\right), \quad (13)$$

and the moment densities ζ_m are expressed as

$$\zeta_m = \frac{\pi\rho_{\mathrm{s}}}{6}\sum_{k=1}^{N_{\mathrm{G}}} x_{\mathrm{s},k} d_{kk}^m, \quad m = 0, 1, 2, 3, \quad (14)$$

where the effective hard-sphere diameter d_{kk} of the reference fluid (cf. Eq. (10)) is used. The summation of Eq. (14) is expressed in terms of the fraction $x_{\mathrm{s},k}$ of segments of a group of type k in the mixture, which is defined as

$$x_{\mathrm{s},k} = \frac{\sum_{i=1}^{N_{\mathrm{C}}} x_i \nu_{k,i}\nu_k^* S_k}{\sum_{i=1}^{N_{\mathrm{C}}} x_i \sum_{l=1}^{N_{\mathrm{G}}} \nu_{l,i}\nu_l^* S_l}. \quad (15)$$

After substituting the expression of the group fraction $x_{\mathrm{s},k}$ (Eq. (15)) in the definition of the reduced densities (Eq. (14)) and expressing the reference expression per segment as a function of the molecular density, one obtains the following expression for the hard-sphere Helmholtz free energy per molecule:

$$\frac{A^{\mathrm{HS}}}{Nk_{\mathrm{B}}T} = \frac{6}{\pi\rho}\left[\left(\frac{\zeta_2^3}{\zeta_3^2} - \zeta_0\right)\ln(1-\zeta_3) + 3\frac{\zeta_1\zeta_2}{1-\zeta_3} + \frac{\zeta_2^3}{\zeta_3(1-\zeta_3)^2}\right], \quad (16)$$

which is identical to the form of the Helmholtz free energy of a hard-sphere mixture.

The first-order term A_1 of the perturbation expansion corresponds to the mean-attractive energy and, as for the hard-sphere term, it is obtained as a summation of the contributions to the mean-attractive energy per segment a_1:

$$\frac{A_1}{Nk_{\mathrm{B}}T} = \frac{1}{k_{\mathrm{B}}T}\left(\sum_{i=1}^{N_{\mathrm{C}}} x_i \sum_{k=1}^{N_{\mathrm{G}}} \nu_{k,i}\nu_k^* S_k\right) a_1. \quad (17)$$

The mean-attractive energy per segment is obtained by summing the pairwise interactions $a_{1,kl}$ between groups k and l over all types of functional groups present in the system,

$$a_1 = \sum_{k=1}^{N_{\mathrm{G}}}\sum_{l=1}^{N_{\mathrm{G}}} x_{\mathrm{s},k} x_{\mathrm{s},l} a_{1,kl}, \quad (18)$$

where it can be shown[73] that

$$a_{1,kl} = \mathcal{C}_{kl}\left[x_{0,kl}^{\lambda_{kl}^{\mathrm{a}}}\left(a_{1,kl}^{\mathrm{s}}(\rho_{\mathrm{s}};\lambda_{kl}^{\mathrm{a}}) + B_{kl}(\rho_{\mathrm{s}};\lambda_{kl}^{\mathrm{a}})\right) - x_{0,kl}^{\lambda_{kl}^{\mathrm{r}}}\left(a_{1,kl}^{\mathrm{s}}(\rho_{\mathrm{s}};\lambda_{kl}^{\mathrm{r}}) + B_{kl}(\rho_{\mathrm{s}};\lambda_{kl}^{\mathrm{r}})\right)\right]. \quad (19)$$

Here, $\mathcal{C}_{kl}$ is the pre-factor of the potential (cf. Eq. (2)), $x_{0,kl}$ is defined as $x_{0,kl} = \sigma_{kl}/d_{kl}$, and B_{kl} is given by

$$B_{kl}(\rho_{\mathrm{s}};\lambda_{kl}) = 2\pi\rho_{\mathrm{s}} d_{kl}^3 \epsilon_{kl}\left[\frac{1-\zeta_{\mathrm{x}}/2}{(1-\zeta_{\mathrm{x}})^3} I(\lambda_{kl}) - \frac{9\zeta_{\mathrm{x}}(1+\zeta_{\mathrm{x}})}{2(1-\zeta_{\mathrm{x}})^3} J(\lambda_{kl})\right]. \quad (20)$$

This expression is written using a generalized notation where the parameter λ_{kl} indicates that the expression can be evaluated for both the repulsive $\lambda_{kl}^{\mathrm{r}}$ and the attractive $\lambda_{kl}^{\mathrm{a}}$ exponents. In Eq. (20) ζ_{x} is the packing fraction of a hypothetical pure fluid of diameter d_{x}, obtained by applying the van der Waals (vdW) one-fluid mixing rule,

$$d_{\mathrm{x}}^3 = \sum_{k=1}^{N_{\mathrm{G}}}\sum_{l=1}^{N_{\mathrm{G}}} x_{\mathrm{s},k} x_{\mathrm{s},l} d_{kl}^3, \quad (21)$$

so that

$$\zeta_{\mathrm{x}} = \frac{\pi\rho_{\mathrm{s}}}{6}\sum_{k=1}^{N_{\mathrm{G}}}\sum_{l=1}^{N_{\mathrm{G}}} x_{\mathrm{s},k} x_{\mathrm{s},l} d_{kl}^3. \quad (22)$$

The unlike effective hard-sphere diameter d_{kl} is obtained with an appropriate combining rule (cf. Sec. III E). The quantities $I(\lambda_{kl})$ and $J(\lambda_{kl})$ are introduced in order to simplify the integration of the potential so as to obtain analytical expressions for the first-order perturbation term as discussed in detail in Ref. 73. Both $I(\lambda_{kl})$ and $J(\lambda_{kl})$ are functions of the parameters of the intermolecular interaction potential alone and are calculated (for either $\lambda_{kl}^{\mathrm{r}}$ or $\lambda_{kl}^{\mathrm{a}}$) as[73]

$$I(\lambda_{kl}) = \int_1^{x_{0,kl}} \frac{x^2}{x^{\lambda_{kl}}}\mathrm{d}x = \frac{1 - x_{0,kl}^{(3-\lambda_{kl})}}{(\lambda_{kl}-3)}, \quad (23)$$

and

$$J(\lambda_{kl}) = \int_1^{x_{0,kl}} \frac{x^3 - x^2}{x^{\lambda_{kl}}}\mathrm{d}x = \frac{1 - x_{0,kl}^{(4-\lambda_{kl})}(\lambda_{kl}-3) + x_{0,kl}^{(3-\lambda_{kl})}(\lambda_{kl}-4)}{(\lambda_{kl}-3)(\lambda_{kl}-4)}. \quad (24)$$

The free energy $a_{1,kl}^{\mathrm{s}}(\rho_{\mathrm{s}};\lambda_{kl})$ appearing in Eq. (19) corresponds to the first-order perturbation term of a Sutherland fluid characterized by a hard-core diameter d_{kl}, an interaction exponent λ_{kl}, and energy well-depth ϵ_{kl}. The exact evaluation of this term requires a knowledge of the radial distribution function of the hard-sphere system over a range of separations. In order to derive an analytical expression in the same spirit as in the original SAFT-VR approach,[109,110] the mean-value theorem is applied in order to integrate over the radial distribution function by mapping it to its value at contact d_{kl} at an effective packing fraction $\zeta_{\mathrm{x}}^{\mathrm{eff.}}$. This procedure is shown to provide a description which is in excellent agreement with

the evaluation of $a^{\mathrm{s}}_{1,kl}(\rho_{\mathrm{s}};\lambda_{kl})$ by full quadrature using an integral equation theory for the radial distribution function.[73] The $a^{\mathrm{s}}_{1,kl}(\rho_{\mathrm{s}};\lambda_{kl})$ term is then evaluated as

$$a^{\mathrm{s}}_{1,kl}(\rho_{\mathrm{s}};\lambda_{kl}) = -2\pi\rho_{\mathrm{s}}\left(\frac{\epsilon_{kl}d^3_{kl}}{\lambda_{kl}-3}\right)\frac{1-\zeta_{\mathrm{x}}^{\mathrm{eff.}}/2}{(1-\zeta_{\mathrm{x}}^{\mathrm{eff.}})^3}. \tag{25}$$

The effective packing fraction has been parameterized[73] for ranges of the exponents of $5 < \lambda_{kl} \leq 100$ and can be expressed as a function of the vdW one-fluid packing fraction ζ_{x} as

$$\zeta_{kl}^{\mathrm{eff.}} = c_{1,kl}\zeta_{\mathrm{x}} + c_{2,kl}\zeta_{\mathrm{x}}^2 + c_{3,kl}\zeta_{\mathrm{x}}^3 + c_{4,kl}\zeta_{\mathrm{x}}^4, \tag{26}$$

where the coefficients ($c_{1,kl}$, $c_{2,kl}$, $c_{3,kl}$, $c_{4,kl}$) are obtained as functions of the exponent λ_{kl} from

$$\begin{pmatrix} c_{1,kl} \\ c_{2,kl} \\ c_{3,kl} \\ c_{4,kl} \end{pmatrix} = \begin{pmatrix} 0.81096 & 1.7888 & -37.578 & 92.284 \\ 1.0205 & -19.341 & 151.26 & -463.50 \\ -1.9057 & 22.845 & -228.14 & 973.92 \\ 1.0885 & -6.1962 & 106.98 & -677.64 \end{pmatrix} \times \begin{pmatrix} 1 \\ 1/\lambda_{kl} \\ 1/\lambda_{kl}^2 \\ 1/\lambda_{kl}^3 \end{pmatrix}. \tag{27}$$

The second-order perturbation term of the high-temperature expansion (cf. Eq. (9)) represents the fluctuation of the attractive energy in the system and is obtained as

$$\frac{A_2}{Nk_{\mathrm{B}}T} = \left(\frac{1}{k_{\mathrm{B}}T}\right)^2\left(\sum_{i=1}^{N_{\mathrm{C}}}x_i\sum_{k=1}^{N_{\mathrm{G}}}\nu_{k,i}\nu_k^*S_k\right)a_2, \tag{28}$$

where the fluctuation term per segment a_2 is obtained from the appropriate sum of the contributions of the pairwise interactions $a_{2,kl}$ between groups k and l as

$$a_2 = \sum_{k=1}^{N_{\mathrm{G}}}\sum_{l=1}^{N_{\mathrm{G}}}x_{\mathrm{s},k}x_{\mathrm{s},l}a_{2,kl}. \tag{29}$$

The expression for a_2 is obtained based on the improved macroscopic compressibility approximation (MCA) proposed by Zhang *et al.*[111] combined with a correction in the same spirit as that proposed by Paricaud[106] for soft potentials. The final expression for $a_{2,kl}$ is given by

$$\begin{aligned} a_{2,kl} = \frac{1}{2}K^{\mathrm{HS}}(1+\chi_{kl})\epsilon_{kl}\mathcal{C}_{kl}^2\Big\{ & x_{0,kl}^{2\lambda_{kl}^{\mathrm{a}}}\left[a^{\mathrm{s}}_{1,kl}\left(\rho_{\mathrm{s}};2\lambda_{kl}^{\mathrm{a}}\right)\right. \\ & \left. + B_{kl}\left(\rho_{\mathrm{s}};2\lambda_{kl}^{\mathrm{a}}\right)\right] \\ & - 2x_{0,kl}^{(\lambda_{kl}^{\mathrm{a}}+\lambda_{kl}^{\mathrm{r}})}\left[a^{\mathrm{s}}_{1,kl}\left(\rho_{\mathrm{s}};\lambda_{kl}^{\mathrm{a}}+\lambda_{kl}^{\mathrm{r}}\right)\right. \\ & \left. + B_{kl}\left(\rho_{\mathrm{s}};\lambda_{kl}^{\mathrm{a}}+\lambda_{kl}^{\mathrm{r}}\right)\right] \\ & + x_{0,kl}^{2\lambda_{kl}^{\mathrm{r}}}\left[a^{\mathrm{s}}_{1,kl}\left(\rho_{\mathrm{s}};2\lambda_{kl}^{\mathrm{r}}\right)+B_{kl}\left(\rho_{\mathrm{s}};2\lambda_{kl}^{\mathrm{r}}\right)\right]\Big\}, \end{aligned} \tag{30}$$

where K^{HS} is the isothermal compressibility of the hypothetical vdW one-fluid (vdW-1) system (with the packing fraction ζ_{x} of Eq. (22)), and is obtained from the Carnahan and Starling hard-sphere expression[112] as

$$K^{\mathrm{HS}} = \frac{(1-\zeta_{\mathrm{x}})^4}{1+4\zeta_{\mathrm{x}}+4\zeta_{\mathrm{x}}^2-4\zeta_{\mathrm{x}}^3+\zeta_{\mathrm{x}}^4}. \tag{31}$$

The correction factor χ_{kl} is obtained from[73]

$$\chi_{kl} = f_1(\alpha_{kl})\zeta_{\mathrm{x}}^* + f_2(\alpha_{kl})(\zeta_{\mathrm{x}}^*)^5 + f_3(\alpha_{kl})(\zeta_{\mathrm{x}}^*)^8, \tag{32}$$

where the quantities f_m, for $m = 1, 2, 3$, as given in Eq. (39), are functions of α_{kl}, a dimensionless form of the integrated van der Waals energy of the Mie potential:

$$\begin{aligned} \alpha_{kl} &= \frac{1}{\epsilon_{kl}\sigma_{kl}^3}\int_{\sigma}^{\infty}\Phi_{kl}^{\mathrm{Mie}}(r)r^2\mathrm{d}r \\ &= \mathcal{C}_{kl}\left(\frac{1}{\lambda_{kl}^{\mathrm{a}}-3}-\frac{1}{\lambda_{kl}^{\mathrm{r}}-3}\right). \end{aligned} \tag{33}$$

Note that in Eq. (32) a quantity ζ_{x}^* is used (not to be confused with ζ_{x} defined in Eq. (22)) which is the packing fraction of a hypothetical pure fluid of diameter σ_{x}. The diameter σ_{x} is obtained based on a vdW one-fluid mixing rule (cf. Eq. (21)) as

$$\sigma_{\mathrm{x}}^3 = \sum_{k=1}^{N_{\mathrm{G}}}\sum_{l=1}^{N_{\mathrm{G}}}x_{\mathrm{s},k}x_{\mathrm{s},l}\sigma_{kl}^3, \tag{34}$$

so that the packing fraction ζ_{x}^* is now defined as

$$\zeta_{\mathrm{x}}^* = \frac{\pi\rho_{\mathrm{s}}}{6}\sum_{k=1}^{N_{\mathrm{G}}}\sum_{l=1}^{N_{\mathrm{G}}}x_{\mathrm{s},k}x_{\mathrm{s},l}\sigma_{kl}^3. \tag{35}$$

The third-order perturbation term is obtained from the contribution per segment a_3 as

$$\frac{A_3}{Nk_{\mathrm{B}}T} = \left(\frac{1}{k_{\mathrm{B}}T}\right)^3\left(\sum_{i=1}^{N_{\mathrm{C}}}x_i\sum_{k=1}^{N_{\mathrm{G}}}\nu_{k,i}\nu_k^*S_k\right)a_3, \tag{36}$$

where a_3 is obtained by summing the pairwise segment-segment contributions $a_{3,kl}$ on groups k and l as previously for the a_1 and a_2 terms:

$$a_3 = \sum_{k=1}^{N_{\mathrm{G}}}\sum_{l=1}^{N_{\mathrm{G}}}x_{\mathrm{s},k}x_{\mathrm{s},l}a_{3,kl}. \tag{37}$$

The contribution $a_{3,kl}$, is obtained using the following empirical expression[73]

$$\begin{aligned} a_{3,kl} = & -\epsilon_{kl}^3 f_4(\alpha_{kl})\zeta_{\mathrm{x}}^*\exp\left[f_5(\alpha_{kl})\zeta_{\mathrm{x}}^*\right. \\ & \left. + f_6(\alpha_{kl})(\zeta_{\mathrm{x}}^*)^2\right]. \end{aligned} \tag{38}$$

A temperature dependence of the $a_{3,kl}$ term is avoided by expressing it as a function of ζ_{x}^*, as opposed to the packing fraction ζ_{x} which has an implicit temperature dependence through the effective diameter d_{kl}.

TABLE I. Coefficients $\phi_{m,n}$ for the $a_{2,kl}$ term (Eq. (32)), the $a_{3,kl}$ term (Eq. (38)), and $\gamma_{c,ii}$ of the g_2 term (Eq. (59)). N/A denotes that no value is required.

n	$\phi_{1,n}$	$\phi_{2,n}$	$\phi_{3,n}$	$\phi_{4,n}$	$\phi_{5,n}$	$\phi_{6,n}$	$\phi_{7,n}$
0	7.5365557	− 359.44	1550.9	− 1.19932	− 1911.28	9236.9	10
1	− 37.60463	1825.6	− 5070.1	9.063632	21390.175	− 129430	10
2	71.745953	− 3168.0	6534.6	− 17.9482	− 51320.7	357230	0.57
3	− 46.83552	1884.2	− 3288.7	11.34027	37064.54	− 315530	− 6.7
4	− 2.467982	− 0.82376	− 2.7171	20.52142	1103.742	1390.2	− 8
5	− 0.50272	− 3.1935	2.0883	− 56.6377	− 3264.61	− 4518.2	N/A
6	8.0956883	3.7090	0	40.53683	2556.181	4241.6	N/A

The functions f_m for $(m = 1, \ldots, 6)$ appearing in Eqs. (32) and (38) are determined from[73]

$$f_m(\alpha_{kl}) = \frac{\sum_{n=0}^{3} \phi_{m,n} \alpha_{kl}^n}{1 + \sum_{n=4}^{6} \phi_{m,n} \alpha_{kl}^{n-3}}, \; m = 1, \ldots, 6\,. \tag{39}$$

The values of the coefficients $\phi_{m,n}$ are listed in Table I. The coefficients that appear in the modified MCA expression for the $a_{2,kl}$ term, i.e., f_m for $m = 1, 2, 3$, were obtained from an analysis of the Monte Carlo simulation data for the fluctuation term and pure-component vapor-liquid equilibrium data of selected Mie fluids (λ^r,λ^a).[73] The coefficients employed for the calculation of the $a_{3,\,kl}$ term were obtained in order to best reproduce the simulation data for vapor-liquid equilibrium data and critical points of the selected Mie (λ^r,λ^a) fluids as explained in Ref. 73. It is important to note that the coefficients included in the calculation of the $a_{3,kl}$ are obtained from simulation data of the fluid-phase behavior of monomers, and as a consequence the final expression for the free energy effectively incorporates higher-order terms of the perturbation expansion of Barker and Henderson[104] (in fact, for the complete series), rather than just the third-order term. A retrospective analysis of the third-order perturbation term has shown that calculations using the empirical expression of Eq. (38) are in good agreement with evaluations of the equivalent term obtained from molecular simulation,[73] which indicates that the series is convergent and terms beyond the third-order make a reduced contribution to the Helmholtz free energy.

C. Chain term

The treatment of the contribution to the free energy due to the formation of molecules from fused Mie segments is undertaken following a formal TPT1 treatment, where the contact value of the radial distribution function at an effective average diameter is required.[66,67] An alternative treatment has been proposed by Peng *et al.*,[70] and later employed in the work of Paduszyński and Domańska,[71] where the chain contribution is calculated using the segment-segment contact values of the RDF. In that way the connectivity of the molecule is retained in the theoretical description. However, as shown in the Appendix, both the RDF of a chain with an average diameter used in our current work and the segment-segment contact approach[70,71] reproduce the thermodynamic behavior of tangentially bonded heteronuclear molecules with similar accuracy in comparison with simulation data.

In order to apply the SAFT-γ treatment of the chain contribution, average molecular parameters ($\bar{\sigma}_{ii}$, $\bar{d}_{ii}$, $\bar{\epsilon}_{ii}$, and $\bar{\lambda}_{ii}$) for each molecular species i in the mixture are introduced;[66,67] this allows for the evaluation of the radial distribution function at a molecularly averaged effective distance. The averaging of the molecular size and energy parameters is independent of the composition of the mixture and makes use of the molecular fraction $z_{k,i}$ of a given group k on a molecule i:

$$z_{k,i} = \frac{\nu_{k,i}\, \nu_k^* S_k}{\sum_{l=1}^{N_G} \nu_{l,i}\, \nu_l^* S_l}\,. \tag{40}$$

The quantity $z_{k,i}$ is not to be confused with the fraction $x_{s,k}$ of a given group k in the mixture, which is composition dependent (cf. Eq. (15)). The average molecular segment size $\bar{\sigma}_{ii}$ and the effective hard-sphere diameter $\bar{d}_{ii}$ of component i are defined as

$$\bar{\sigma}_{ii}^3 = \sum_{k=1}^{N_G} \sum_{l=1}^{N_G} z_{k,i} z_{l,i} \sigma_{kl}^3, \tag{41}$$

and

$$\bar{d}_{ii}^3 = \sum_{k=1}^{N_G} \sum_{l=1}^{N_G} z_{k,i} z_{l,i} d_{kl}^3. \tag{42}$$

The averaging rule for the effective hard-sphere diameter $\bar{d}_{ii}$ is chosen such that the value of the vdW one-fluid packing fraction of a mixture of *heteronuclear* monomeric segments, as calculated in Eq. (22), is the same when calculated for monomeric segments of average molecular size $\bar{d}_{ii}$, i.e.,

$$\begin{aligned}\zeta_x &= \frac{\pi \rho_s}{6} \sum_{k=1}^{N_G} \sum_{l=1}^{N_G} x_{s,k} x_{s,l} d_{kl}^3 \\ &= \frac{\pi \rho_s}{6} \sum_{i=1}^{N_C} \sum_{j=1}^{N_C} x_i \left(\sum_{k=1}^{N_G} \nu_k^* \nu_{k,i} S_k \right) x_j \left(\sum_{k=1}^{N_G} \nu_k^* \nu_{k,j} S_k \right) \bar{d}_{ij}^3.\end{aligned} \tag{43}$$

Other effective molecular parameters are obtained in the same way, so that the average interaction energy $\bar{\epsilon}_{ii}$ and exponents $\bar{\lambda}_{ii}$ which characterize the potential are obtained as

$$\bar{\epsilon}_{ii} = \sum_{k=1}^{N_G} \sum_{l=1}^{N_G} z_{k,i} z_{l,i} \epsilon_{kl}, \tag{44}$$

and

$$\bar{\lambda}_{ii} = \sum_{k=1}^{N_G}\sum_{l=1}^{N_G} z_{k,i} z_{l,i} \lambda_{kl}. \tag{45}$$

Relation (45) holds for both the repulsive, $\bar{\lambda}^{r}_{ii}$, and the attractive, $\bar{\lambda}^{a}_{ii}$, exponents.

The contribution to the free energy of the mixture due to the formation of a chain of tangent or fused segments is based on the first-order perturbation theory (TPT1) of Wertheim[47–50,52] but using the effective molecular parameters:

$$\frac{A^{\text{chain}}}{N k_B T} = -\sum_{i=1}^{N_C} x_i \sum_{k=1}^{N_G} (\nu_{k,i}\nu_k^* S_k - 1) \ln g_{ii}^{\text{Mie}}(\bar{\sigma}_{ii}; \zeta_x), \tag{46}$$

where $g_{ii}^{\text{Mie}}(\bar{\sigma}_{ii}; \zeta_x)$ is the value of the RDF of the hypothetical one-fluid Mie system at a packing fraction ζ_x evaluated at the effective diameter $\bar{\sigma}_{ii}$. An accurate estimate of the contact value of the RDF for a Mie fluid can be obtained by means of a second-order expansion:[73]

$$g_{ii}^{\text{Mie}}(\bar{\sigma}_{ii}; \zeta_x) = g_d^{\text{HS}}(\bar{\sigma}_{ii}) \exp\left[\beta\bar{\epsilon}_{ii} g_1(\bar{\sigma}_{ii})/g_d^{\text{HS}}(\bar{\sigma}_{ii}) + (\beta\bar{\epsilon}_{ii})^2 g_2(\bar{\sigma}_{ii})/g_d^{\text{HS}}(\bar{\sigma}_{ii})\right]. \tag{47}$$

The zeroth-order term of the expansion, $g_d^{\text{HS}}(\bar{\sigma}_{ii})$, is the radial distribution function of a system of hard spheres of diameter $\bar{d}_{ii}$ evaluated at distance $\bar{\sigma}_{ii}$ (and packing fraction ζ_x). As shown in Ref. 73, an expression for this function can be obtained following Boublík's[113] recipe:

$$g_d^{\text{HS}}(\bar{\sigma}_{ii}) = \exp\left(k_0 + k_1 \bar{x}_{0,ii} + k_2 \bar{x}_{0,ii}^2 + k_3 \bar{x}_{0,ii}^3\right), \tag{48}$$

which is valid for $1 < \bar{x}_{0,ii} < \sqrt{2}$ (with $\bar{x}_{0,ii} = \bar{\sigma}_{ii}/\bar{d}_{ii}$). The coefficients k_m in this expression are obtained as functions of the vdW one-fluid packing fraction ζ_x (cf. Eq. (22)) of the hypothetical pure fluid as

$$k_0 = -\ln(1-\zeta_x) + \frac{42\zeta_x - 39\zeta_x^2 + 9\zeta_x^3 - 2\zeta_x^4}{6(1-\zeta_x)^3}, \tag{49}$$

$$k_1 = \frac{\zeta_x^4 + 6\zeta_x^2 - 12\zeta_x}{2(1-\zeta_x)^3}, \tag{50}$$

$$k_2 = \frac{-3\zeta_x^2}{8(1-\zeta_x)^2}, \tag{51}$$

and

$$k_3 = \frac{-\zeta_x^4 + 3\zeta_x^2 + 3\zeta_x}{6(1-\zeta_x)^3}. \tag{52}$$

The first-order term $g_1(\bar{\sigma}_{ii})$ of the expansion for the contact value of the RDF (cf. Eq. (47)) is approximated by its value at the contact distance $\bar{d}_{ii}$, obtained by means of a self-consistent method for the calculation of pressure from the virial and the free-energy routes[73,109,110] so that

$$g_1(\bar{\sigma}_{ii}) \approx g_1(\bar{d}_{ii}) = \frac{1}{2\pi\bar{\epsilon}_{ii}\bar{d}_{ii}^3}\left[3\frac{\partial \bar{a}_{1,ii}}{\partial \rho_s} - \bar{C}_{ii}\bar{\lambda}^{a}_{ii}\bar{x}_{0,ii}^{\bar{\lambda}^{a}_{ii}} \frac{\bar{a}^{s}_{1,ii}(\rho_s;\bar{\lambda}^{a}_{ii}) + \bar{B}_{ii}(\rho_s;\bar{\lambda}^{a}_{ii})}{\rho_s} + \bar{C}_{ii}\bar{\lambda}^{r}_{ii}\bar{x}_{0,ii}^{\bar{\lambda}^{r}_{ii}} \frac{\bar{a}^{s}_{1,ii}(\rho_s;\bar{\lambda}^{r}_{ii}) + \bar{B}_{ii}(\rho_s;\bar{\lambda}^{r}_{ii})}{\rho_s}\right]. \tag{53}$$

In this expression $\bar{C}_{ii}$ is the prefactor of the effective molecular interaction potential of component i obtained using the values of the average molecular repulsive and attractive exponents ($\bar{\lambda}^{r}_{ii}$ and $\bar{\lambda}^{a}_{ii}$), i.e., $\bar{C}_{ii} = \frac{\bar{\lambda}^{r}_{ii}}{\bar{\lambda}^{r}_{ii}-\bar{\lambda}^{a}_{ii}}\left(\frac{\bar{\lambda}^{r}_{ii}}{\bar{\lambda}^{a}_{ii}}\right)^{\frac{\bar{\lambda}^{a}_{ii}}{\bar{\lambda}^{r}_{ii}-\bar{\lambda}^{a}_{ii}}}$. The quantity $\bar{B}_{ii}(\rho_s;\bar{\lambda}_{ii})$ is obtained using Eq. (20) as

$$\bar{B}_{ii}(\rho_s;\bar{\lambda}_{ii}) = 2\pi\rho_s\bar{d}_{ii}^3\bar{\epsilon}_{ii}\left[\frac{1-\zeta_x/2}{(1-\zeta_x)^3}\bar{I}(\bar{\lambda}_{ii}) - \frac{9\zeta_x(1+\zeta_x)}{2(1-\zeta_x)^3}\bar{J}(\bar{\lambda}_{ii})\right], \tag{54}$$

but with $\bar{I}(\bar{\lambda}_{ii})$ and $\bar{J}(\bar{\lambda}_{ii})$ (cf. Eqs. (23) and (24)) now based on the effective exponents $\bar{\lambda}^{r}_{ii}$ and $\bar{\lambda}^{a}_{ii}$ and the ratio $\bar{x}_{0,ii} = \bar{\sigma}_{ii}/\bar{d}_{ii}$.

The first-order term of the radial distribution function further depends on the density derivative of the effective first-order perturbation term $\bar{a}_{1,ii}$ for the contribution of the monomeric interactions to the free energy per segment, which is calculated from expression (19) as

$$\bar{a}_{1,ii} = \bar{C}_{ii}\left[\bar{x}_{0,ii}^{\bar{\lambda}^{a}_{ii}}\left(\bar{a}^{s}_{1,ii}(\rho_s;\bar{\lambda}^{a}_{ii}) + \bar{B}_{ii}(\rho_s;\bar{\lambda}^{a}_{ii})\right) - \bar{x}_{0,ii}^{\bar{\lambda}^{r}_{ii}}\left(\bar{a}^{s}_{1,ii}(\rho_s;\bar{\lambda}^{r}_{ii}) + \bar{B}_{ii}(\rho_s;\bar{\lambda}^{r}_{ii})\right)\right]. \tag{55}$$

The integrated energy of the Sutherland fluid $\bar{a}^{s}_{1,ii}(\rho_s;\bar{\lambda}_{ii})$ calculated for the effective molecular parameters is obtained as

$$\bar{a}^{s}_{1,ii}(\rho_s;\bar{\lambda}_{ii}) = -2\pi\rho_s\left(\frac{\bar{\epsilon}_{ii}\bar{d}_{ii}^3}{\bar{\lambda}_{ii}-3}\right)\frac{1-\bar{\zeta}_{ii}^{\text{eff.}}/2}{\left(1-\bar{\zeta}_{ii}^{\text{eff.}}\right)^3}, \tag{56}$$

where the effective packing fraction $\bar{\zeta}_{ii}^{\text{eff.}}$ used for the mapping of the radial distribution function at contact is now calculated as

$$\bar{\zeta}_{ii}^{\text{eff.}} = \bar{c}_{1,ii}\zeta_x + \bar{c}_{2,ii}\zeta_x^2 + \bar{c}_{3,kl}\zeta_x^3 + \bar{c}_{4,ii}\zeta_x^4. \tag{57}$$

The coefficients of Eq. (57) are obtained based on the averaged values of the exponents of the potential ($\bar{\lambda}_{ii}$):

$$\begin{pmatrix} \bar{c}_{1,ii} \\ \bar{c}_{2,ii} \\ \bar{c}_{3,ii} \\ \bar{c}_{4,ii} \end{pmatrix} = \begin{pmatrix} 0.81096 & 1.7888 & -37.578 & 92.284 \\ 1.0205 & -19.341 & 151.26 & -463.50 \\ -1.9057 & 22.845 & -228.14 & 973.92 \\ 1.0885 & -6.1962 & 106.98 & -677.64 \end{pmatrix} \times \begin{pmatrix} 1 \\ 1/\bar{\lambda}_{ii} \\ 1/\bar{\lambda}_{ii}^2 \\ 1/\bar{\lambda}_{ii}^3 \end{pmatrix}. \quad (58)$$

The second-order term $g_2(\bar{\sigma}_{ii})$ of Eq. (47) is also approximated by its value at the effective diameter $\bar{d}_{ii}$. It is obtained based on the expression of the macroscopic compressibility approximation and an empirical correction:[73]

$$g_2(\bar{\sigma}_{ii}) \approx g_2(\bar{d}_{ii}) = (1 + \gamma_{c,ii}) g_2^{\mathrm{MCA}}(\bar{d}_{ii}). \quad (59)$$

The correction factor $\gamma_{c,ii}$ is given as a function of temperature, the one-fluid packing fraction ζ_x^* (see Eq. (35)), and the averaged values of the exponents of the potential as

$$\gamma_{c,ii} = \phi_{7,0}\{-\tanh[\phi_{7,1}(\phi_{7,2} - \bar{\alpha}_{ii})] + 1\} \times \zeta_x^* \theta \exp(\phi_{7,3}\zeta_x^* + \phi_{7,4}(\zeta_x^*)^2), \quad (60)$$

where $\theta = \exp(\beta\bar{\epsilon}_{ii}) - 1$, the values of the coefficients $\phi_{7,0}$, …, $\phi_{7,4}$ are given in Table I, and $\bar{\alpha}_{ii}$ is obtained from the molecular averaged exponents of the potential (cf. Eq. (33)) as

$$\bar{\alpha}_{ii} = \bar{C}_{ii}\left(\frac{1}{\bar{\lambda}_{ii}^{\mathrm{a}} - 3} - \frac{1}{\bar{\lambda}_{ii}^{\mathrm{r}} - 3}\right). \quad (61)$$

The second-order term from the macroscopic compressibility approximation $g_2^{\mathrm{MCA}}(\bar{d}_{ii})$ of Eq. (59) is obtained based on the fluctuation term of the Sutherland potential as

$$g_2^{\mathrm{MCA}}(\bar{d}_{ii}) = \frac{1}{2\pi\bar{\epsilon}_{ii}^2\bar{d}_{ii}^3}\left[3\frac{\partial}{\partial\rho_s}\left(\frac{\bar{a}_{2,ii}}{1+\bar{\chi}_{ii}}\right) - \bar{\epsilon}_{ii}K^{\mathrm{HS}}\bar{C}_{ii}^2\bar{\lambda}_{ii}^{\mathrm{r}}\bar{x}_{0,ii}^{2\bar{\lambda}_{ii}^{\mathrm{r}}}\frac{\bar{a}_{1,ii}^{\mathrm{s}}(\rho_s;2\bar{\lambda}_{ii}^{\mathrm{r}}) + \bar{B}(\rho_s;2\bar{\lambda}_{ii}^{\mathrm{r}})}{\rho_s} + \bar{\epsilon}_{ii}K^{\mathrm{HS}}\bar{C}_{ii}^2(\bar{\lambda}_{ii}^{\mathrm{r}} + \bar{\lambda}_{ii}^{\mathrm{a}})\bar{x}_{0,ii}^{(\bar{\lambda}_{ii}^{\mathrm{r}}+\bar{\lambda}_{ii}^{\mathrm{a}})} \times \frac{\bar{a}_{1,ii}^{\mathrm{s}}(\rho_s;\bar{\lambda}_{ii}^{\mathrm{r}} + \bar{\lambda}_{ii}^{\mathrm{a}}) + \bar{B}(\rho_s;\bar{\lambda}_{ii}^{\mathrm{r}} + \bar{\lambda}_{ii}^{\mathrm{a}})}{\rho_s} - \bar{\epsilon}_{ii}K^{\mathrm{HS}}\bar{C}_{ii}^2\bar{\lambda}_{ii}^{\mathrm{a}}\bar{x}_{0,ii}^{2\bar{\lambda}_{ii}^{\mathrm{a}}}\frac{\bar{a}_{1,ii}^{\mathrm{s}}(\rho_s;2\bar{\lambda}_{ii}^{\mathrm{a}}) + \bar{B}(\rho_s;2\bar{\lambda}_{ii}^{\mathrm{a}})}{\rho_s}\right]. \quad (62)$$

where all of the parameters and free energy terms are evaluated using the effective molecular parameters. Note that the empirical correction to the MCA expression is based on the molecular parameters:

$$\bar{\chi}_{ii} = f_1(\bar{\alpha}_{ii})\zeta_x^* + f_2(\bar{\alpha}_{ii})(\zeta_x^*)^5 + f_3(\bar{\alpha}_{ii})(\zeta_x^*)^8, \quad (63)$$

where the coefficients f_1, f_2, f_3 are obtained from Eq. (39) by using $\bar{\alpha}_{ii}$ instead of α_{kl}.

D. Association term

The contribution to the Helmholtz free energy arising from the association of molecules due to the bonding sites is obtained in the Wertheim TPT1 form as[47–50,52,53]

$$\frac{A^{\mathrm{assoc.}}}{Nk_BT} = \sum_{i=1}^{N_C} x_i \sum_{k=1}^{N_G} \nu_{k,i} \sum_{a=1}^{N_{ST,k}} n_{k,a}\left(\ln X_{i,k,a} + \frac{1 - X_{i,k,a}}{2}\right), \quad (64)$$

where $N_{ST,k}$ is the total number of site types on a given group k, and $n_{k,a}$ is the number of sites of type a on group k. $X_{i,k,a}$ represents the fraction of molecules of component i that are not bonded at a site of type a on group k. It is obtained from the solution of the mass action equation as[50,53,66]

$$X_{i,k,a} = \frac{1}{1 + \sum_{j=1}^{N_C}\sum_{l=1}^{N_G}\sum_{b=1}^{N_{ST,l}} \rho x_j \nu_{l,j} n_{l,b} X_{j,l,b}\Delta_{ij,kl,ab}}. \quad (65)$$

Here, $\Delta_{ij,kl,ab}$ characterizes the association strength between a site of type a on a group of type k of component i and a site of type b on a group of type l of component j. By introducing the square-well bonding potential and carrying out an angle average, the following expression can be obtained:[53]

$$\Delta_{ij,kl,ab} = \bar{\sigma}_{ij}^3 F_{kl,ab} I_{kl,ab}, \quad (66)$$

where $F_{kl,ab} = \exp(\epsilon_{kl,ab}^{\mathrm{HB}}/k_BT) - 1$, and $I_{kl,ab}$ is a dimensionless integral defined as[73]

$$I_{kl,ab} = \frac{\pi}{6\bar{\sigma}_{ij}^3(r_{kl,ab}^{\mathrm{d}})^2}\int_{(2r_{kl,ab}^{\mathrm{d}} - r_{kl,ab}^{\mathrm{c}})}^{(2r_{kl,ab}^{\mathrm{d}} + r_{kl,ab}^{\mathrm{c}})} g^{\mathrm{Mie}}(r) \times (r_{kl,ab}^{\mathrm{c}} + 2r_{kl,ab}^{\mathrm{d}} - r)^2(2r_{kl,ab}^{\mathrm{c}} - 2r_{kl,ab}^{\mathrm{d}})r\mathrm{d}r. \quad (67)$$

The determination of the integral in Eq. (67) requires an expression for the RDF of the reference Mie fluid over a range of distances. For a detailed discussion of the various options on how the integral can be evaluated, see Refs. 73 and 114. For example, the RDF can be approximated based on a Barker-Henderson zeroth-order perturbation approach, so that $g^{\mathrm{Mie}}(r) \simeq g_d^{\mathrm{HS}}(r)$. After assuming that $r^2 g_d^{\mathrm{HS}}(r) \simeq d^2 g_d^{\mathrm{HS}}(d)$, a compact analytical form for the association contribution can be obtained, so that the integral of Eq. (67) can be expressed as

$$I_{kl,ab} \approx g_d^{\mathrm{HS}}(\bar{d}_{ij}) K_{ij,kl,ab}. \quad (68)$$

The bonding volume $K_{ij,kl,ab}$ is obtained from[73]

$$K_{ij,kl,ab} = \frac{\pi \bar{d}_{ij}^2}{18\bar{\sigma}_{ij}^3 r_{kl,ab}^{\mathrm{d}\,2}} \Big[\ln\left(\left(r_{kl,ab}^{\mathrm{c}} + 2r_{kl,ab}^{\mathrm{d}}\right)/\bar{d}_{ij}\right) \times \left(6\left(r_{kl,ab}^{\mathrm{c}}\right)^3 + 18\left(r_{kl,ab}^{\mathrm{c}}\right)^2 r_{kl,ab}^{\mathrm{d}} - 24\left(r_{kl,ab}^{\mathrm{d}}\right)^3\right) + \left(r_{kl,ab}^{\mathrm{c}} + 2r_{kl,ab}^{\mathrm{d}} - \bar{d}_{ij}\right)\left(22\left(r_{kl,ab}^{\mathrm{d}}\right)^2 - 5r_{kl,ab}^{\mathrm{c}} r_{kl,ab}^{\mathrm{d}} - 7r_{kl,ab}^{\mathrm{d}}\bar{d}_{ij} - 8\left(r_{kl,ab}^{\mathrm{c}}\right)^2 + r_{kl,ab}^{\mathrm{c}}\bar{d}_{ij} + \bar{d}_{ij}^2\right)\Big]. \tag{69}$$

The value of the radial distribution function at contact, $g_d^{\mathrm{HS}}(\bar{d}_{ij})$, is readily available from the expression of Boublík:[107]

$$g_d^{\mathrm{HS}}(\bar{d}_{ij}) = \frac{1}{1-\zeta_3} + 3\frac{\bar{d}_{ii}\bar{d}_{jj}}{\bar{d}_{ii}+\bar{d}_{jj}}\frac{\zeta_2}{(1-\zeta_3)^2} + 2\left(\frac{\bar{d}_{ii}\bar{d}_{jj}}{\bar{d}_{ii}+\bar{d}_{jj}}\right)^2 \frac{\zeta_2^2}{(1-\zeta_3)^3}. \tag{70}$$

E. Combining rules

Combining rules for the unlike intermolecular parameters are commonly employed within equations of state to facilitate the study of binary and multicomponent systems. In the specific case of the methodology presented in our current work, the interactions between groups of different type also contribute to the description of pure components when represented with a *heteronuclear* molecular model. The unlike segment diameter is obtained from a simple arithmetic mean (Lorentz rule[115]) as

$$\sigma_{kl} = \frac{\sigma_{kk} + \sigma_{ll}}{2}, \tag{71}$$

and the same combining rule is applied for the calculation of the unlike effective hard-sphere diameter, so that d_{kl} is calculated as

$$d_{kl} = \frac{d_{kk} + d_{ll}}{2}. \tag{72}$$

Bearing in mind the definition of the Barker and Henderson hard-sphere diameter (cf. Eq. (10)), a more rigorous way to obtain d_{kl} would be to integrate the potential of the unlike interaction between groups k and l as

$$d_{kl} = \int_0^{\sigma_{kl}} \left[1 - \exp\left\{-\frac{\Phi_{kl}^{\mathrm{Mie}}(r_{kl})}{k_{\mathrm{B}}T}\right\}\right] \mathrm{d}r. \tag{73}$$

However, such an approach would require extensive numerical calculations. Moreover, in agreement with earlier findings,[73] the approximation of d_{kl} as an arithmetic mean is found to have minimal impact on the performance of the method, as judged by the quality of the description of the properties of real compounds.

The unlike dispersion energy ϵ_{kl} between groups k and l, can be obtained by applying an augmented geometric mean rule, which also accounts for the asymmetry in size:

$$\epsilon_{kl} = \frac{\sqrt{\sigma_{kk}^3\sigma_{ll}^3}}{\sigma_{kl}^3}\sqrt{\epsilon_{kk}\epsilon_{ll}}. \tag{74}$$

The combining rule for the repulsive λ_{kl}^r and the attractive λ_{kl}^a exponents of the unlike interaction is obtained by invoking the geometric mean for the integrated van der Waals energy of a Sutherland fluid,

$$\alpha_{\mathrm{vdW},kl}^{\mathrm{s}} = 2\pi\epsilon_{kl}\sigma_{kl}^3\left(\frac{1}{\lambda_{kl}-3}\right), \tag{75}$$

and by imposing the Berthelot condition,[115] $\alpha_{\mathrm{vdW},kl}^{\mathrm{s}} = \sqrt{\alpha_{\mathrm{vdW},kk}^{\mathrm{s}}\alpha_{\mathrm{vdW},ll}^{\mathrm{s}}}$, which results in

$$\lambda_{kl} = 3 + \sqrt{(\lambda_{kk}-3)(\lambda_{ll}-3)}. \tag{76}$$

The combining rule of Eq. (74) provides a first estimate of the value of the unlike dispersion energy. It is known, however, that real systems often exhibit large deviations from simple or augmented combining rules, especially when the molecules comprise chemically different components and groups. As will be discussed in Secs. IV and V, the unlike dispersion energy ϵ_{kl} often has to be treated as an adjustable parameter in practice.

In the case of associating compounds, the unlike range of the association site-site interaction is obtained as

$$r_{kl,ab}^{\mathrm{c}} = \frac{r_{kk,aa}^{\mathrm{c}} + r_{ll,bb}^{\mathrm{c}}}{2}. \tag{77}$$

The unlike value of the association energy can be obtained by means of a simple geometric mean rule:

$$\epsilon_{kl,ab}^{\mathrm{HB}} = \sqrt{\epsilon_{kk,aa}^{\mathrm{HB}}\epsilon_{ll,bb}^{\mathrm{HB}}}. \tag{78}$$

However, typically $\epsilon_{kl,ab}^{\mathrm{HB}}$ is treated as an adjustable parameter, and is estimated by regression to experimental data.

A number of combining rules for the average molecular parameters required for the calculation of the chain and association contributions to the free energy also need to be considered. The unlike values for the effective segment size, $\bar{\sigma}_{ij}$ and $\bar{d}_{ij}$, dispersion energy, $\bar{\epsilon}_{ij}$, and repulsive and attractive exponents of the potential, $\bar{\lambda}_{ij}$, are obtained from

$$\bar{\sigma}_{ij} = \frac{\bar{\sigma}_{ii} + \bar{\sigma}_{jj}}{2}, \tag{79}$$

$$\bar{d}_{ij} = \frac{\bar{d}_{ii} + \bar{d}_{jj}}{2}, \tag{80}$$

$$\bar{\epsilon}_{ij} = \frac{\sqrt{\bar{\sigma}_{ii}^3\bar{\sigma}_{jj}^3}}{\bar{\sigma}_{ij}^3}\sqrt{\bar{\epsilon}_{ii}\bar{\epsilon}_{jj}}, \tag{81}$$

and

$$\bar{\lambda}_{ij} = 3 + \sqrt{(\bar{\lambda}_{ii}-3)(\bar{\lambda}_{jj}-3)}. \tag{82}$$

Once the functional form of the Helmholtz free energy has been specified other properties, such as the pressure p, chemical potential (or activity) of each component μ_i, internal energy u, enthalpy h, entropy S, Gibbs free energy G, and second-order derivative properties including the isochoric c_{V} and isobaric c_{p} heat capacities, the speed of sound u, isothermal compressibility k_{T}, thermal expansion coefficient α, and Joule-Thomson coefficient μ_{JT} can be obtained algebraically from the standard thermodynamic relations.[116] In order to determine the fluid-phase equilibria the conditions of thermal,

mechanical, and chemical equilibria are solved by ensuring that the temperature, pressure, and chemical potential of each component are equal in each phase and that the state corresponds to a global minimum in the Gibbs free energy (e.g., see Ref. 117).

IV. ESTIMATION OF GROUP PARAMETERS

The parameters that describe the contribution of each functional group to the molecular properties are typically estimated from appropriate experimental data. In our SAFT-γ Mie approach, the compounds are modeled as heteronuclear molecules formed from distinct functional (chemical) groups, and each non-associating group is fully characterized by the following set of parameters (cf. Sec. II for more details): the number of segments ν_k^*, the shape factor S_k, the segment diameter σ_{kk}, the dispersion energy ϵ_{kk}, and the repulsive $\lambda_{kk}^{\mathrm{r}}$ and attractive $\lambda_{kk}^{\mathrm{a}}$ exponents of the potential. The number of segments comprising a group is determined by examining the different realistic possibilities with a trial-and-error approach, and the rest of the group parameters are estimated from appropriate experimental data.

As discussed in Sec. III E, the unlike segment diameter, σ_{kl}, and the values of the exponents of the unlike interaction potential, $\lambda_{kl}^{\mathrm{r}}$ and $\lambda_{kl}^{\mathrm{a}}$, are calculated by means of the combining rules given in Eqs. (71) and (76), respectively. The value of the unlike dispersion energy ϵ_{kl} is typically treated as an adjustable parameter and is therefore obtained by regression to experimental data. In many cases, the value of the unlike interaction energy can be estimated from pure-component data as will be shown in Sec. V. This is a unique characteristic of heteronuclear models; this can be used to provide accurate predictions for properties of mixtures from pure component data alone. Mixture data are also used where necessary to estimate the unlike energy, as was demonstrated in previous work.[68]

The group parameters are estimated from experimental data for a series of pure substances belonging to a given chemical family. In most group contribution approaches, one first considers the *n*-alkane series in the parameter estimation procedure, where the parameters for the methyl (CH_3) and the methylene (CH_2) groups are obtained. Once the parameters for these groups have been determined, they are transferred to the representation of compounds with additional functional groups based on experimental data for the corresponding homologous series, e.g., the *n*-alkyl esters for the carboxylate (COO) group. The parameters that describe each functional group in the SAFT-γ Mie EoS are obtained by regression to pure-component vapor-liquid equilibrium data (i.e., vapor pressures p_{vap}, and saturated liquid densities ρ_{sat}), as well as single-phase densities $\rho_{\mathrm{liq}}(T, p)$ at given temperatures and pressures. The temperature range commonly used for vapor-liquid equilibrium data is between the triple point and $0.9T_{\mathrm{crit}}^{\mathrm{exp}}$, with $T_{\mathrm{crit}}^{\mathrm{exp}}$ representing the experimental critical temperature of the substance under study. Experimental data closer than $0.9T_{\mathrm{crit}}^{\mathrm{exp}}$ are not included in the parameter estimation in our current work, despite the improved description of the near-critical region with the novel methodology. Since the equation of state is a classical theory it is characterized by mean-field critical exponents and does not allow one to reproduce the density fluctuations in the critical region; including data closer to the critical point would bias the parameters towards a more accurate representation of the critical point and therefore result in a loss of their physical significance. This would in turn make the extrapolation to other thermodynamic conditions less reliable. For the single-phase density, experimental data at high temperatures and pressures in the liquid and supercritical regions are typically used. These data are included when available as they provide information on the compressibility of the fluid and can help achieve an accurate prediction of derivative thermodynamic properties. The objective function used in the parameter estimation procedure is

$$\begin{aligned}\min_{\boldsymbol{\Omega}} f_{\mathrm{obj}} = w_1 \sum_{u=1}^{N_{p_{\mathrm{vap}}}} \left[\frac{p_{\mathrm{vap}}^{\mathrm{exp}}(T_u) - p_{\mathrm{vap}}^{\mathrm{calc}}(T_u; \boldsymbol{\Omega})}{p_{\mathrm{vap}}^{\mathrm{exp}}(T_u)} \right]^2 \\ + w_2 \sum_{v=1}^{N_{\rho_{\mathrm{sat}}}} \left[\frac{\rho_{\mathrm{sat}}^{\mathrm{exp}}(T_v) - \rho_{\mathrm{sat}}^{\mathrm{calc}}(T_v; \boldsymbol{\Omega})}{\rho_{\mathrm{sat}}^{\mathrm{exp}}(T_v)} \right]^2 \\ + w_3 \sum_{y=1}^{N_{\rho_{\mathrm{liq}}}} \left[\frac{\rho_{\mathrm{liq}}^{\mathrm{exp}}(T_y, p_y) - \rho_{\mathrm{liq}}^{\mathrm{calc}}(T_y, p_y; \boldsymbol{\Omega})}{\rho_{\mathrm{liq}}^{\mathrm{exp}}(T_y, p_y)} \right]^2, \end{aligned} \tag{83}$$

where $\boldsymbol{\Omega}$ denotes the vector of the parameters to be estimated, the indices u, v, and y allow for the summations over all experimental (exp) points for each property, denoted as $N_{p_{\mathrm{vap}}}$, $N_{\rho_{\mathrm{sat}}}$, and $N_{\rho_{\mathrm{liq}}}$ for the vapor pressure, saturated liquid density, and single-phase density, respectively. The desired level of accuracy for each calculated (calc) property can be adjusted by means of weighting factors: w_1 for p_{vap}, w_2 for ρ_{sat}, and w_3 for ρ_{liq}; in our current work, $w_1 = w_2 = w_3 = 1$ is used. The estimations are performed using the commercial software package gPROMS©.[118] Multiple starting points are used as input to local optimizations, carried out using a gradient-based successive quadratic programming algorithm.[118]

V. RESULTS AND DISCUSSION

A. SAFT-γ Mie group parameters

In the first instance models for the characterization of the functional groups of two chemical families are developed within our novel SAFT-γ Mie framework: the *n*-alkanes and *n*-alkyl esters. In Secs. V A 1 and V A 2, the development of models for the functional groups for each chemical family, together with the detailed results of the regression to the experimental data are presented. The metric used in our work to quantify the accuracy of the theoretical description of the experimental data for a property R of a given compound is the percentage average absolute deviation (%AAD) defined as

$$\%\mathrm{AAD}R = \frac{1}{n_R} \sum_{i=1}^{n_R} \left| \frac{R_i^{\mathrm{exp.}} - R_i^{\mathrm{calc.}}}{R_i^{\mathrm{exp.}}} \right|, \tag{84}$$

where n_R is the number of data points of a property, $R_i^{\mathrm{exp.}}$ is the experimental value, and $R_i^{\mathrm{calc.}}$ is the calculated value for the same property at the conditions of the *i*th experimental point.

TABLE II. Group parameters for the methyl and methylene functional groups (CH_3 and CH_2) and the carboxylate functional group (COO) within the SAFT-γ Mie group contribution approach.

Functional group k	v_k^*	S_k	λ_{kk}^r	λ_{kk}^a	σ_{kk} [Å]	ϵ_{kk}/k_B [K]
CH_3	1	0.57255	15.050	6	4.0772	256.77
CH_2	1	0.22932	19.871	6	4.8801	473.39
COO	1	0.65264	31.189	6	3.9939	868.92

1. n-Alkanes

The chemical family of the *n*-alkanes is considered first in order to obtain the model parameters that describe the methyl (CH_3) and methylene (CH_2) functional groups. The parameters estimated for these functional groups, summarized in Tables II and III, are estimated from experimental data for the vapor pressure, saturated liquid density, and single-phase density of linear alkanes from ethane to *n*-decane. The number of data points and the temperature range (and pressure range for the single-phase density) for each compound and property considered are reported in Table IV.

The quality of the description of the pure-component vapor-liquid equilibria of the *n*-alkanes included in the regression is depicted for the coexistence densities in Figure 2(a) and for the vapor pressure in Figure 2(b). From the figures it can be seen that the SAFT-γ Mie group contribution approach allows for an excellent description of the phase behavior of the correlated compounds, from ethane to *n*-decane. The deviations (%AAD) from the experimental data for the vapor pressure and saturated liquid density are summarized in Table IV. The average deviation for all correlated *n*-alkanes was found to be 1.55% for p_{vap} and 0.59% for ρ_{sat} and shows a significant improvement when compared to the results obtained by with the SAFT-γ approach for models based on the square-well potential (3.98% for p_{vap} and 0.57% for ρ_{sat}) for the vapor pressure, with a similar performance for the saturated densities.[66] The level of accuracy of the SAFT-γ Mie approach constitutes a clear improvement in the description of the pure-component phase behavior of the *n*-alkanes when compared to other group contribution approaches within SAFT: Tamouza *et al.*[31] have reported average deviations of 2.63% for the vapor pressure and 2.29% for the saturated liquid density with their homonuclear GC approach based on the SAFT-0,[119] and 1.66% and 2.23% with that based on SAFT-VR SW;[109,110] in the case of the hetero GC-SAFT-VR of Peng *et al.*[70] deviations of 5.95% and 3.07% are reported for the vapor pressure and saturated liquid density, respectively. The deviations with our SAFT-γ Mie approach are similar to the hs PC-SAFT[71] deviations of 0.96% for p_{vap} and 0.56% for ρ_{sat}, which are obtained for a smaller temperature range, namely, from 0.5 to $0.9T_{crit}^{exp}$. It should be noted, however, that though a comparison of the deviations of different methods provides a measure of the accuracy of each approach, these are based on different experimental data and temperature ranges, as well as, in some cases, different sets of compounds.

TABLE III. Unlike dispersion interaction energies ϵ_{kl} for the methyl and methylene functional groups of CH_3 and CH_2 and the carboxylate functional group of COO within the SAFT-γ Mie group contribution approach.

ϵ_{kl}/k_B [K]	CH_3	CH_2	COO
CH_3	256.77	350.77	402.75
CH_2	350.77	473.39	498.86
COO	402.75	498.86	868.92

The deviations reported here are based on data within a temperature range up to $0.9T_{crit}^{exp}$ and as such fail to express the improved performance of the SAFT-γ Mie approach in the description of the near-critical region of pure substances. The improvement can be appreciated when comparing graphically the vapor-liquid equilibria of selected *n*-alkanes obtained with our SAFT-γ Mie approach and the corresponding SAFT-γ SW version[66] (cf. Figure 3). From the comparison, it can be clearly seen that the SAFT-γ Mie EoS provides a significantly improved description of the near-critical region of systems with varying chain length, decreasing the overshoot of the critical point whilst retaining a highly accurate description of the fluid-phase behavior at temperatures far from the critical point. We reiterate that the approach, being an analytical mean-field type theory, fails to reproduce the critical scaling observed experimentally. An accurate representation of the critical properties would require the application of a renormalization group treatment, e.g., as applied to the SAFT-VR EoS.[91,120,121]

The description of the *n*-alkane single-phase densities ρ_{liq} (cf. Table IV) is also excellent, with an average deviation for all compounds of 0.59%. When examining each compound it can be seen that the highest deviations are observed for ethane, as was also observed for the SAFT-γ SW approach.[66] One may argue that ethane should not be included in the parameter estimation procedure, since ethane does not contain a CH_3–CH_2 interaction, while all longer *n*-alkanes do. Furthermore, group contribution techniques are generally not well suited to the study of small molecules as proximity effects are neglected. With this in mind the procedure was repeated omitting the data for ethane and the inclusion of these experimental data was not found to bias the parameters of the groups in a way that would result in a sub-optimal description for the higher *n*-alkanes. When a more accurate model is needed, ethane can be described as a separate functional group (e.g., as would be the case for water, methanol, etc.). This strategy has been followed within the hetero GC-SAFT-VR of Peng *et al.*[70] and the GC-SAFT of Tamouza *et al.*[31] where *n*-propane was the first molecule considered in the series for the estimation of the parameters for the *n*-alkanes.

As has already been mentioned, a particular advantage of the Mie potential is that the detailed form of the pair interaction potential between segments can be modified by adjusting the values of the repulsive and attractive exponents. This allows one to capture the finer features of the interaction which are important in providing an accurate description of the thermodynamic derivative properties. For the parameters that determine the form of the interaction potential between the CH_3 and CH_2 functional groups, the value of the attractive exponent is fixed to $\lambda_{kk}^a = 6$ for both groups. This choice is based on a consideration of the chemical na-

TABLE IV. Percentage average absolute deviations (%AAD) for the vapor pressures $p_{vap}(T)$, saturated liquid densities $\rho_{sat}(T)$, and single-phase densities $\rho_{liq}(T, p)$ of the *n*-alkanes obtained with the SAFT-γ Mie group contribution approach with respect to the correlated experimental data from NIST,[146] where *n* is the number of data points.

Compound	*T* range [K]	*n*	%AAD $p_{vap}(T)$	*T* range [K]	*n*	%AAD $\rho_{sat}(T)$	*T* range [K]	*p* range [MPa]	*n*	%AAD $\rho_{liq}(T, p)$
C_2H_6	125–275	31	2.24	125–275	31	1.48	150–550	10–50	123	0.96
n-C_3H_8	147–332	38	2.22	147–332	38	0.74	150–500	10–50	108	0.49
n-C_4H_{10}	170–385	44	1.27	170–385	44	0.37	150–550	10–50	123	0.50
n-C_5H_{12}	187–422	48	1.90	187–422	48	0.36	150–550	10–50	120	0.60
n-C_6H_{14}	201–456	52	1.68	201–456	52	0.27	188–548	10–50	108	0.52
n-C_7H_{16}	216–486	55	1.01	216–486	55	0.46	193–553	10–50	108	0.62
n-C_8H_{18}	227–512	58	1.22	227–512	58	0.54	226–546	10–50	95	0.64
n-C_9H_{20}	237–532	60	0.69	237–532	60	0.59	230–550	10–50	95	0.50
n-$C_{10}H_{22}$	245–555	63	1.75	245–555	63	0.52	253–553	10–50	89	0.47
Average	...	...	1.55	...	...	0.59	...	...	...	0.59

ture of the groups, which, considering their apolar nature, are expected to interact via London dispersion forces which are characterized by an attractive exponent of six.[43,122] The values of the repulsive exponents estimated from the experimental data for the *n*-alkanes are found to be $\lambda^r_{CH_3,CH_3} = 15.050$ and $\lambda^r_{CH_2,CH_2} = 19.871$. Potoff and Bernard-Brunel[123] have developed a force field for the methyl and methylene groups based on the Mie potential for use as force fields in molecular simulation (Monte Carlo/molecular dynamics) of the fluid-phase behavior of *n*-alkanes, finding that a good description can be obtained with values of the repulsive exponent of 16 for both groups. The values of the shape factors for the CH_3 and CH_2 groups are also determined from the parameter estimation procedure. The optimal values obtained are $S_{CH_3} = 0.57255$ and $S_{CH_2} = 0.22932$, which are found to be quite different from those used in previous work with the square-well potential.[66] In the previous study, the shape factors for the CH_3 and CH_2 groups were fixed to 1/3 and 2/3, respectively, as these yield the molecular aspect ratio typically used to represent the *n*-alkanes in a homonuclear model.[57,124–126] The segment size of the CH_3 group is found to be smaller than the size of the CH_2 group (4.0772 Å compared to 4.8801 Å), which is in line with the smaller value of the shape factor for the CH_2 group. Comparing the values of the segment

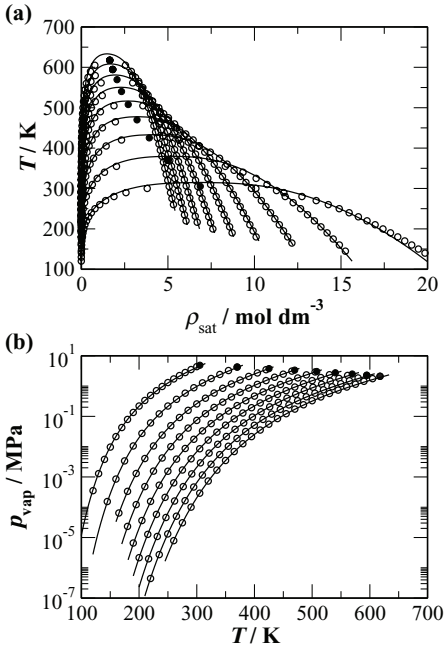

FIG. 2. The description with the SAFT-γ Mie group contribution approach of the fluid-phase equilibria of the *n*-alkanes included in the estimation of the methyl CH_3 and methylene CH_2 parameters: (a) the coexistence densities ρ_{sat} (*n*-ethane to *n*-decane from bottom to top); and (b) the vapor pressures p_{vap} in a logarithmic representation (*n*-ethane to *n*-decane from left to right). The open symbols represent the experimental data, the filled symbols the corresponding experimental critical points[146] and the continuous curves the calculations with the theory.

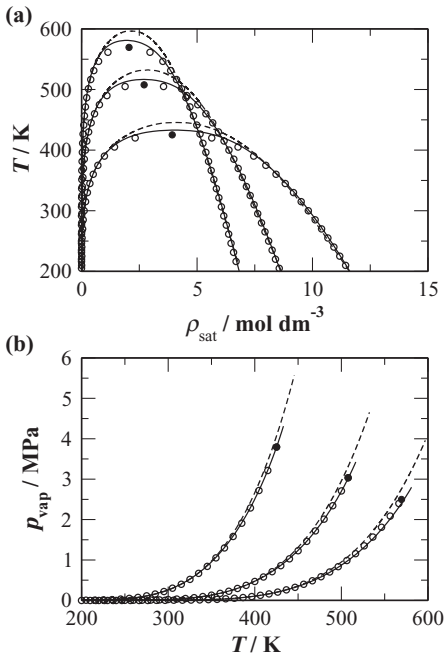

FIG. 3. Comparison of the description with the SAFT-γ SW[66] (dashed curves) and SAFT-γ Mie (continuous curves) group contribution approaches of the pure-component vapor-liquid equilibria of *n*-butane, *n*-hexane, and *n*-octane: (a) coexistence densities ρ_{sat} (from bottom to top); and (b) vapor pressures p_{vap} (from left to right). The open symbols represent the experimental data and the filled symbols the corresponding experimental critical points.[146]

TABLE V. Percentage average absolute deviations (%AAD) for the vapor pressures $p_{vap}(T)$, saturated liquid densities $\rho_{sat}(T)$, and single-phase densities $\rho_{liq}(T, p)$ of the *n*-alkyl esters obtained with the SAFT-γ Mie group contribution approach with respect to the experimental data, where *n* is the number of data points.

Compound	*T* range [K]	*n*	%AAD $p_{vap}(T)$	Ref.	*T* range [K]	*n*	%AAD $\rho_{sat}(T)$	Ref.	*T* range [K]	*p* range [MPa]	*n*	Ref.	%AAD $\rho_{liq}(T, p)$
$CH_3COOCH_2CH_3$	307–473	29	0.37	[147, 148]	273–473	21	0.25	[147]	298–393	1 - 20	80	[149]	0.43
$CH_3COO(CH_2)_2CH_3$	303–493	20	0.49	[150]	303–493	20	0.17	[150]	298–393	1 - 20	80	[149]	0.43
$CH_3COO(CH_2)_3CH_3$	334–399	27	0.73	[151]	298–523	25	0.42	[149, 152]	298–393	1 - 20	80	[149]	0.19
$CH_3COO(CH_2)_4CH_3$	321–462	23	0.85	[153]	298–393	20	0.18	[149]	298–393	1 - 20	80	[149]	0.19
$CH_3COO(CH_2)_5CH_3$	274–459	33	1.86	[154]	273–431	18	0.24	[155]	…	…	…	…	…
$CH_3COO(CH_2)_6CH_3$	274–478	30	0.67	[154, 155]	273–428	19	0.20	[155]	…	…	…	…	…
Average	…	…	0.83	…	…	…	0.24	…	…	…	…	…	0.31

diameters to the ones obtained with SAFT-γ SW,[66] one finds a significant increase; this will be discussed in more detail when the predictions of the theory for longer *n*-alkanes including the polyethylene polymer limit are examined in Sec. V B 1.

2. n-Alkyl esters

Having determined the parameters for the CH_3 and CH_2 functional groups, these can be transferred in the description of other homologous series of compounds to determine the parameters of additional functional groups. In the current work we develop parameters for the COO group, and its interactions with the CH_3 and CH_2 groups, based on experimental data for selected *n*-alkyl acetates. A number of different GC schemes have been suggested to represent these compounds: in the modified UNIFAC (Dortmund) approach an acetyl (CH_3COO) functional group is employed;[127] in the case of SAFT-based group contribution methods, a carboxylate COO group is used in the work of Thi *et al.*[34] with the homonuclear GC-SAFT approach, and Peng *et al.*[70] employ a methoxyl CH_3O group (in conjunction with a carbonyl C=O group) in the framework of the hetero GC-SAFT-VR approach. In our work the COO group is treated as comprising one segment ($\nu^*_{COO} = 1$) and is modeled as non-associating, as esters are not expected to self-associate. Association sites will have to be included in order to capture the unlike association in some polar mixtures containing esters and, e.g., water or alkanols (cf. the work of Kleiner and Sadowski[128]). Here, we treat the polarity of the esters implicitly through the variable interaction range of the potential. A more explicit treatment of the polar nature of these molecules can be followed by including an additional polar term in the free energy, as in the work of Thi *et al.*,[34] or alternatively by the incorporation of two association sites.

In our case the value of the attractive exponent is fixed to the London $\lambda^a_{COO,COO} = 6$, as for the groups of the *n*-alkanes, and the remaining parameters are estimated based on regression to a compilation of pure-component and mixture experimental data. The pure-component data used include experimental data for the saturated liquid density, vapor pressure, and single-phase liquid density for ethyl acetate to *n*-heptyl acetate; data for methyl acetate was not included in the regression, as typically within GC approaches the first member of a chemical family is treated separately (e.g., methanol, methane, etc.). The specifics of the temperature and pressure ranges, the number of points for each property, as well as the deviations for each property and each compound are given in Table V; the corresponding estimated parameters are presented in Tables II and III. In addition to the pure-component data, experimental data for the enthalpies of mixing of two binary *n*-alkyl acetate + *n*-alkane mixtures have been included in the parameter estimation: ethyl acetate + *n*-hexane, and *n*-butyl acetate + *n*-octane. The corresponding objective function is given in Eq. (83) with an additional term accounting for the deviation between the experimental and the calculated value of the enthalpy of mixing for a given composition of each mixture where weights of $w_1 = w_2 = w_3 = 1$ and $w_1 = 0.04$ are used in this case:

$$\begin{aligned}\min_{\mathbf{\Omega}} f_{\text{obj}} &= w_1 \sum_{u=1}^{N_{p\text{vap}}} \left[\frac{p^{\text{exp}}_{\text{vap}}(T_u) - p^{\text{calc}}_{\text{vap}}(T_u; \mathbf{\Omega})}{p^{\text{exp}}_{\text{vap}}(T_u)} \right]^2 \\ &+ w_2 \sum_{v=1}^{N_{\rho\text{sat}}} \left[\frac{\rho^{\text{exp}}_{\text{sat}}(T_v) - \rho^{\text{calc}}_{\text{sat}}(T_v; \mathbf{\Omega})}{\rho^{\text{exp}}_{\text{sat}}(T_v)} \right]^2 \\ &+ w_3 \sum_{y=1}^{N_{\rho\text{liq}}} \left[\frac{\rho^{\text{exp}}_{\text{liq}}(T_y, p_y) - \rho^{\text{calc}}_{\text{liq}}(T_y, p_y; \mathbf{\Omega})}{\rho^{\text{exp}}_{\text{liq}}(T_y, p_y)} \right]^2 \\ &+ w_4 \sum_{z=1}^{N_{h^E}} \left[\frac{h^{\text{E,exp}}(T_z, p_z, x_z) - h^{\text{E,calc}}(T_z, p_z, x_z; \mathbf{\Omega})}{h^{\text{E,exp}}(T_z, p_z, x_z)} \right]^2. \end{aligned} \tag{85}$$

Experimental data for selected mixtures are included in the estimation procedure so as to have a more complete characterization of the unlike interactions between the alkyl and carboxylate functional groups, to ensure an accurate description of the highly non-ideal phase behavior that these mixtures exhibit, and to increase the statistical significance of the interaction parameters.

A comparison of the SAFT-γ Mie description with the experimental data is given for the saturated liquid densities in Figure 4(a) and for the vapor pressures in Figure 4(b). The overall deviations (%AAD) for the correlated compounds (cf. Table V) are 0.83% for p_{vap}, 0.24% for ρ_{sat}, and 0.31% for ρ_{liq}. It is evident from the reported deviations and the figures that the SAFT-γ Mie approach leads to an excellent

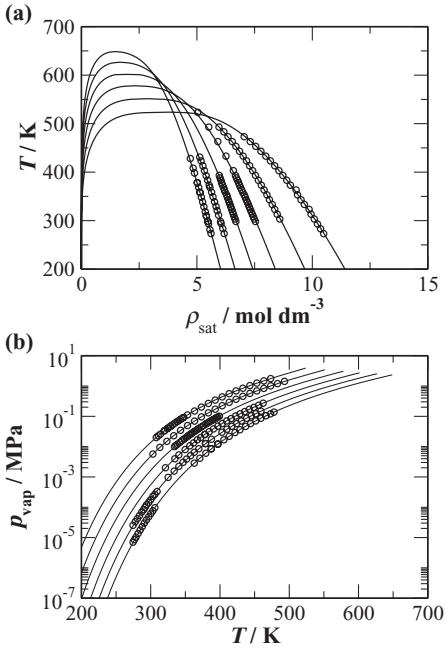

FIG. 4. The description with the SAFT-γ Mie group contribution approach of the fluid-phase equilibria of the *n*-alkyl esters included in the estimation of the carboxylate COO group parameters: (a) the coexistence densities ρ_{sat} (ethyl acetate to *n*-heptyl acetate from bottom to top); and (b) the vapor pressures p_{vap} in a logarithmic representation (ethyl acetate to *n*-heptyl acetate from left to right). The symbols represent experimental data[147–155] and the continuous curves represent the calculations with the theory.

description of the coexistence and single-phase properties of the compounds considered in the parameter estimation procedure. Thi *et al.*[34] have applied three versions of SAFT (the SAFT-0,[119] SAFT-VR,[109,110] and PC-SAFT[129]) combined with a polar term and parameterized the COO functional group (for esters other than formates, HCOOR). The parameters for the COO group were obtained based on a selection of acetates, propanoates, butanoates, and other esters. For the same compounds as the ones used in the development of the SAFT-γ Mie parameters for the COO group presented in our current work, the deviations reported by Thi *et al.* were 4.76%, 3.05%, and 4.20% for p_{vap}, and 1.62%, 1.72%, and 2.87% for ρ_{sat} with the GC-SAFT based on SAFT-0, SAFT-VR, and PC-SAFT, respectively. The performance of the hetero GC-SAFT-VR of Peng *et al.*,[70] where alkyl acetates are modeled by using separate CH_3O and C=O groups is somewhat less accurate with average deviations (from *n*-propyl to *n*-heptyl acetate) of 7.29% for p_{vap} and 2.14% for ρ_{sat}. Although a direct comparison with the other methods is difficult due to the different experimental data used, the reported deviations for each methodology indicate that our new SAFT-γ Mie EoS leads to a significant improvement in the description of the pure-component fluid-phase behavior of *n*-alkyl acetates.

The limited mixture data included in the regression are also well represented with SAFT-γ Mie approach, as shown in Figure 5. The average deviation (%AAD) of the excess enthalpies for the binary systems included in the estimation was found to be 7.37% (8.78% for ethyl acetate + *n*-hexane, and 5.95% for *n*-butyl acetate + *n*-octane), and the level of agreement was deemed satisfactory based on the sensitivity of the

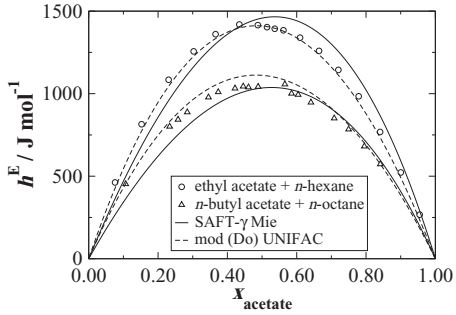

FIG. 5. Excess enthalpies of mixing h^E as a function of the mole fraction *x* of the *n*-alkyl acetate in binary mixtures with *n*-alkanes included in the estimation of the parameters for the carboxylate COO group. The triangles are experimental data for *n*-butyl acetate + *n*-octane at a temperature of T = 298.15 K and pressure of p = 0.1 MPa,[162] and the circles for ethyl acetate + *n*-hexane at T = 318.15 K and p = 0.101325 MPa.[163] The continuous curves are the calculations with the SAFT-γ Mie EoS and the dashed curves are the corresponding calculations with the modified UNIFAC (Dortmund)[127] approach.

selected properties to the unlike interaction parameters between the functional groups and the small values of the excess enthalpies exhibited by these mixtures (~0.5 to 1.5 kJ/mol). In order to assess the level of accuracy, the description of the heat of mixing obtained with the SAFT-γ Mie approach was compared with the corresponding description using modified UNIFAC (Dortmund),[127] where the group parameters were obtained by regression to data for different mixture properties including phase equilibria and excess enthalpies. From the comparison shown in Figure 5, it can be seen that the modified UNIFAC (Dortmund) provides a better description of the experimental excess enthalpies with an average deviation of 3.91%. Bearing in mind that within the modified UNIFAC approach group parameters are exclusively developed to describe (limited) properties of binary and multi-component mixtures, and that within the SAFT-γ Mie approach the primary target is a more complete thermodynamic description of pure components and mixtures, the performance of SAFT-γ Mie in the description of the excess enthalpies is very satisfactory.

The resulting form of the interaction potential of the COO group is described by an optimal value of the repulsive exponent of $\lambda^r_{COO,COO} = 31.189$, which accounts for the nature of the electrostatic interactions of the group in an effective manner. No explicit treatment of the polarity of the esters is included in the model developed in the current work; as mentioned earlier a term accounting for polar interactions has been considered in other modeling approaches for esters,[34] but at the expense of a more complicated description in terms of additional parameters. The estimated value of the segment size of the COO group is $\sigma_{COO,COO} = 3.9939$ Å, which is slightly smaller than the size of the CH_3 group (4.0772 Å), but combined with the larger value of the shape factor ($S_{COO} = 0.65264$ compared to $S_{CH_3} = 0.57255$) corresponds to an overall larger size for the COO group, as expected from the chemical composition of the functional groups. The energy of interaction characterizing the COO group is found to be rather high, $\epsilon_{COO,COO}/k_B = 868.92$ K, which is mainly attributed to the fact that there are two oxygen centers and that the

TABLE VI. Comparison of the percentage average absolute deviations (%AAD) for the isobaric heat capacity $c_p(T, p)$, isochoric heat capacity $c_V(T, p)$, speed of sound $u(T, p)$, isothermal compressibility $k_T(T, p)$, and (volume) thermal expansion coefficient $\alpha_V(T, p)$ of the *n*-alkanes obtained with the SAFT-γ Mie and the SAFT-γ SW[66] group contribution approaches from the correlated experimental data from REFPROP,[130] where n is the number of data points.

				%AAD SAFT-γ Mie					%AAD SAFT-γ SW				
Compound	T range [K]	p range [MPa]	n	$c_p(T, p)$	$c_V(T, p)$	$u(T, p)$	$k_T(T, p)$	$\alpha_V(T, p)$	$c_p(T, p)$	$c_V(T, p)$	$u(T, p)$	$k_T(T, p)$	$\alpha_V(T, p)$
C_2H_6	150–600	10–50	138	3.18	3.76	2.49	3.53	3.50	7.86	10.30	7.42	8.27	9.78
n-C_3H_8	150–600	10–50	138	1.76	0.79	1.31	2.70	3.31	6.98	8.43	4.16	9.65	9.32
n-C_4H_{10}	150–570	10–50	129	1.98	1.92	0.78	1.84	3.70	7.96	11.06	4.48	12.40	10.45
n-C_5H_{12}	150–600	10–50	138	1.83	1.40	1.21	3.16	5.20	7.74	10.30	5.37	15.71	11.21
n-C_6H_{14}	190–600	10–50	124	0.96	1.31	0.82	3.36	5.91	5.33	7.48	4.62	11.55	10.12
n-C_7H_{16}	190–600	10–50	122	0.96	1.54	1.47	4.07	6.44	5.75	8.11	5.93	14.18	10.23
n-C_8H_{18}	230–600	10–50	111	0.59	2.19	0.92	3.45	7.33	4.73	7.51	5.29	12.07	10.61
n-C_9H_{20}	230–600	10–50	110	0.47	1.23	2.08	5.47	6.32	4.83	6.57	6.15	14.56	9.22
n-$C_{10}H_{22}$	260–670	10–50	123	0.42	1.73	2.26	6.25	7.74	3.89	5.56	5.64	12.81	10.57
Average	...	...	...	1.35	1.76	1.48	3.76	5.49	6.12	8.37	5.45	12.36	10.17

polar nature of the COO group is treated implicitly through the dispersion interactions.

B. Predictions

1. Pure components

An assessment of the adequacy of the parameters obtained for the CH_3, CH_2, and COO functional groups can be made by examining the performance of the theory in describing the thermodynamic properties of compounds not included in the parameter estimation procedure. The application of the Mie intermolecular potential was previously shown to allow for an accurate simultaneous description of fluid-phase equilibria and thermodynamic derivative properties[72,73] when cast as a theory for homonuclear models. The prediction of derivative properties is a stringent test in any thermodynamic description, and high deviations are to be expected with most equations of state, be it with traditional cubic EoSs or the SAFT variants based on a fixed form of the intermolecular potential.[72,73] Here, we examine the performance of the SAFT-γ Mie approach in the description of second-order thermodynamic derivative properties of representative *n*-alkanes and *n*-alkyl esters (cf. Tables VI and VII). A comparison of the predictions of our current approach and the corresponding results obtained with the SAFT-γ SW EoS[66] in representing the experimental data from REFPROP[130] for the isobaric and isochoric heat capacities, the speed of sound, the isothermal compressibility, and the thermal expansion coefficient of the linear *n*-alkanes from ethane to *n*-decane is provided in Table VI. For the calculation of caloric and derivative properties, the free energy of the ideal gas is determined based on the GC approach of Joback and Reid[9] for the ideal gas heat capacity, $c_{p,0}$. Though these expressions are based on correlations for a temperature range between 273 and ~1000 K, a reliable description is found when extrapolated to lower temperatures. From Table VI it can be seen that the SAFT-γ Mie EoS provides a very accurate prediction of the second-order thermodynamic derivative properties of the *n*-alkanes examined, and constitutes a significant improvement to the description obtained with the SAFT-γ SW EoS based on the square-well potential.[66] The level of agreement between the predictions of the SAFT-γ Mie theory and the correlated experimental data from REFPROP[130] for the speed of sound, isothermal compressibility, isobaric heat capacity, and thermal expansion coefficient of selected *n*-alkanes at different thermodynamic conditions is also depicted in Figure 6. In Figure 7 the predictions of our SAFT-γ Mie approach are compared to the experimental data for the isochoric heat capacity of selected *n*-alkanes, at conditions both close to and far from the critical point. From Figure 7(a) it is evident that the theory provides an excellent representation of the temperature dependence of the isochoric heat capacity for three prototypical alkanes (*n*-butane, *n*-hexane, and *n*-octane), for both the liquid and the vapor branches, including the discontinuity at the liquid-vapor transition. The description of the pressure dependence of the isochoric heat capacity is depicted in Figure 7(b) for *n*-propane along both sub- and super-critical isotherms. The theory is shown to provide a satisfactory description of the isochoric heat capacity at all conditions; slight deviations are observed for the near-critical isotherm at $T = 350$ K (with $T^{\text{exp}}_{\text{crit},C_3H_8} = 369.89$ K[130]), as well as for the super-critical isotherm at $T = 400$ K. A weak divergence is reproduced by the theory, however an accurate description of the singular behavior of the isochoric heat capacity along the critical isotherm would require a formal renormalization-group treatment.

It is important to reiterate that the calculations presented in this section for the second-order thermodynamic derivative properties of *n*-alkanes are predictions, as no such data were included in developing the parameters that characterize each functional group. The assessment of the performance of the theory for these challenging thermodynamic properties provides a good indication of the physical robustness of the parameters obtained for the CH_3 and CH_2 functional groups. This is of crucial importance as these functional groups constitute the molecular backbone of a wide variety of substances. Given that within the approach used here group parameters are obtained in a sequential manner, it is essential to ensure that high-fidelity parameters have been derived for the methyl and methylene groups.

A key advantage of a group contribution formulation lies in the transferability of the group parameters. In order

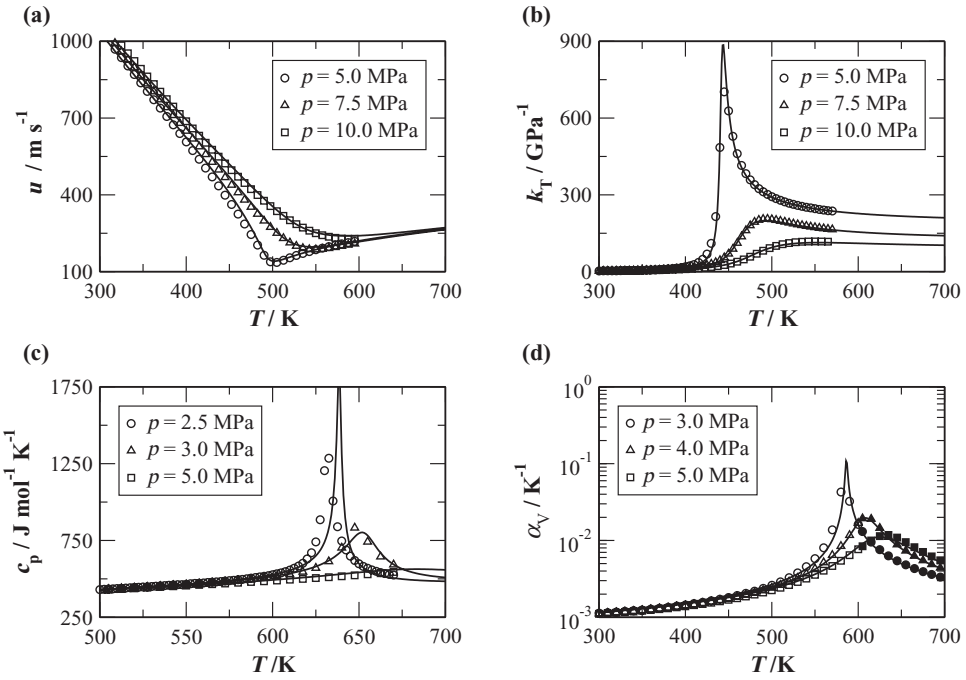

FIG. 6. Prediction of second-order thermodynamic derivative properties of selected *n*-alkanes with the SAFT-γ Mie group contribution approach at various pressures: (a) speed of sound u of *n*-pentane; (b) isothermal compressibility k_T of *n*-butane; (c) isobaric heat capacity c_p of *n*-decane; and (d) (volumetric) thermal expansion coefficient α_V of *n*-octane. The symbols represent correlated experimental data from REFPROP[130] and the continuous curves represent the theoretical predictions. The high-temperature data for *n*-octane shown as filled points in part (d) are based on extrapolations provided by REFPROP that lie outside the temperature range of the correlations.

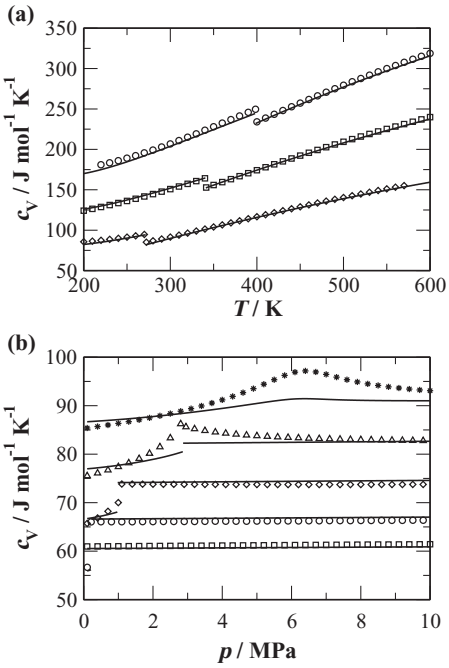

FIG. 7. Comparison of the predictions of the SAFT-γ Mie group contribution approach and the experimental data for the isochoric heat capacity of: (a) *n*-butane (diamonds), *n*-hexane (squares), and *n*-octane (circles) as a function of temperature at a pressure of $p = 0.1$ MPa; and (b) *n*-propane as a function of pressure at a temperature of $T = 200$ K (squares), 250 K (circles), 300 K (diamonds), 350 K (triangles), and 400 K (asterisks). All symbols are correlated experimental data from REFPROP.[130] The continuous curves are the predictions of the theory.

to assess this feature, the parameters for the CH_3 and the CH_2 functional groups are applied to the prediction of pure-component properties of systems not used to estimate the group parameters. Predictions with the SAFT-γ Mie EoS of the fluid-phase behavior for some heavier *n*-alkanes (namely, *n*-pentadecane, *n*-eicosane, *n*-pentacosane, and *n*-triacontane) are compared with the experimental data in Figure 8, and the corresponding deviations are summarized in Table VIII. From this analysis it is clear that the methyl and methylene group parameters can be transferred successfully to the prediction of the pure-component fluid-phase behavior of longer *n*-alkanes; the description of the saturated liquid density remains good, while large deviations are seen for the vapor pressure. The latter could be related to the high uncertainty and low absolute values of the experimental data for the saturation pressure of the higher molecular-weight compounds at low temperatures. Apart from the fluid-phase behavior, the CH_3 and CH_2 group parameters result in a good description of derivative properties of long *n*-alkanes, as shown in Figure 9(a) for the speed of sound of *n*-pentadecane (n-$C_{15}H_{32}$) and Figure 9(b) for the isothermal compressibility of *n*-eicosane (n-$C_{20}H_{42}$). The results obtained with the SAFT-γ Mie approach and the parameters developed for the CH_3 and CH_2 groups show a significant improvement in the prediction of the derivative properties of the long chain *n*-alkanes studied compared to the predictions with the SAFT-γ SW EoS, also included in Figure 9.

The formulation of a SAFT-type approach within a group contribution concept combines the wide range of

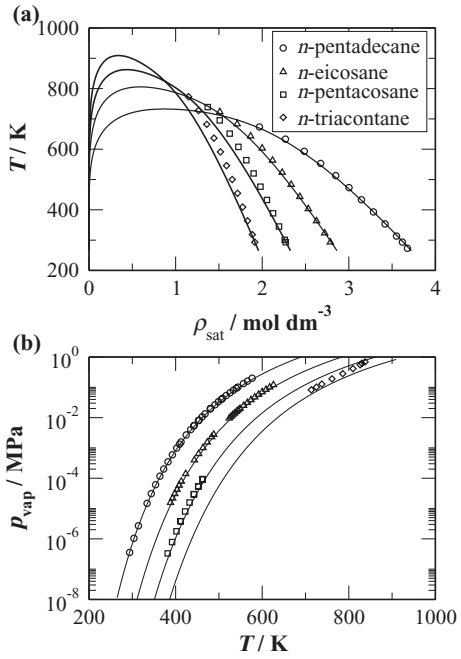

FIG. 8. Comparison of the predictions of the SAFT-γ Mie group contribution approach and the experimental data for the pure-component vapor-liquid equilibria of long-chain *n*-alkanes not included in the estimation of the methyl and methylene group parameters: (a) saturated liquid densities ρ_{sat}; and (b) vapor pressures p_{vap} of *n*-pentadecane (*n*-$C_{15}H_{32}$), *n*-eicosane (*n*-$C_{20}H_{42}$), *n*-pentacosane (*n*-$C_{25}H_{52}$), and *n*-triacontane (*n*-$C_{30}H_{62}$). All symbols are correlated experimental data[152,157–160] and the continuous curves are the predictions of the theory.

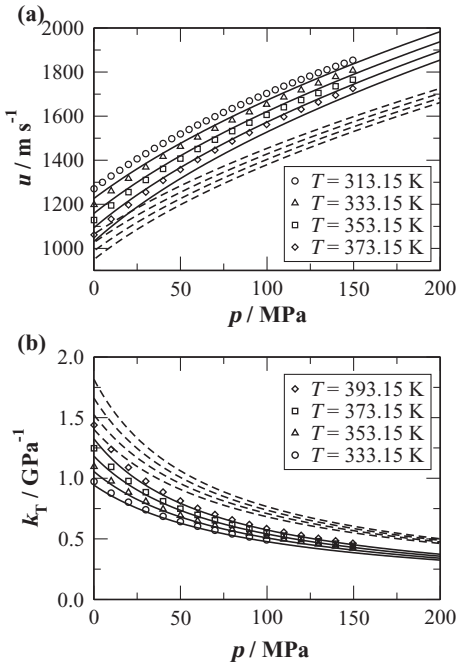

FIG. 9. Comparison of the SAFT-γ Mie (continuous curves) and the SAFT-γ SW[66] (dashed curves) group contribution approaches in the description of second-order thermodynamic derivative properties of long-chain *n*-alkanes not included in the estimation of the group parameters: (a) speed of sound *u* of *n*-pentadecane at temperatures of $T = 313.15$ K (circles), 333.15 K (triangles), 353.15 K (squares), 373.15 K (diamonds);[164] and (b) isothermal compressibility k_T of *n*-eicosane at $T = 333.15$ K (circles), 353.15 K (triangles), 373.15 K (squares), and 393.15 K (diamonds).[165]

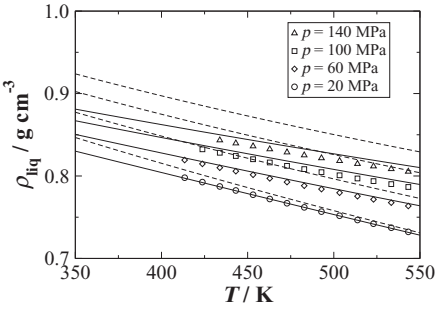

FIG. 10. Comparison of the predictions of the SAFT-γ Mie (continuous curves) and the SAFT-γ SW[66] (dashed curves) group contribution approaches with the experimental data[166] of the single-phase liquid densities ρ_{liq} of linear polyethylene (MW = 126 000 g mol^{-1}) at pressures of p = 20 MPa (circles), 60 MPa (diamonds), 100 MPa (squares), and 140 MPa (triangles).

applicability of EoSs and the predictive nature of GC methods. This can be illustrated in the description of the thermodynamic properties of polymers. The SAFT EoS has been successfully applied as a general methodology to study polymeric systems (e.g., see Refs. 119 and 131–134); the theory is particularly suited to polymers due to the explicit consideration of the chain connectivity. Within the scope of the current work, and taking advantage of the group contribution formulation, the properties of polyethylene polymers can be predicted, using the parameters for the methyl and methylene groups estimated from the experimental data for the lower *n*-alkanes (cf. Sec. V A 1). The predictions of the SAFT-γ Mie approach are compared with the experimental single-phase densities of liquid (molten) linear polyethylene in Figure 10. The parameters for the methyl and (predominantly) for the methylene group are seen to allow for an accurate description of linear polyethylene with a molecular weight of 126 000 g mol^{-1} over a broad range of temperatures and pressures. Achieving this level of agreement with the experimental data is particularly challenging, especially when one recalls that the parameters for the CH_3 and CH_2 groups are developed from the properties of the much shorter *n*-alkanes, ranging from ethane to *n*-decane. The description obtained with the SAFT-γ SW EoS using published parameters[66] is also plotted in Figure 10. From the comparison it is apparent that the representation of the density of polyethylene with Mie segments provides a marked improvement over that obtained with square-well segments, and lends credence to the physical relevance of the parameters for the CH_3 and CH_2 groups (cf. Table II).

A similar assessment is performed for the chemical family of the *n*-alkyl acetates, where the performance of the methodology in the prediction of second-order derivative properties is examined. The deviations of the SAFT-γ Mie predictions from the experimental data for the speed of sound, isobaric and isochoric heat capacities, and isothermal and isentropic compressibilities for selected *n*-alkyl acetates are summarized in Table VII. From the table it can be seen that higher deviations are observed in the description of the thermodynamic derivative properties considered for the lower molecular-weight compounds. This could be due to the dominance of the polar nature of the COO functional group for

TABLE VII. Percentage average absolute deviations (%AAD) for the isobaric heat capacity $c_p(T, p)$, isochoric heat capacity $c_V(T, p)$, speed of sound $u(T, p)$, isothermal compressibility $k_T(T, p)$, and isentropic compressibility $k_S(T, p)$ of selected *n*-alkyl acetates obtained with the SAFT-γ Mie group contribution approach from the experimental data at a pressure of $p = 0.1$ MPa,[156] where n is the number of data points.

			%AAD SAFT-γ Mie				
Compound	T range [K]	n	$c_p(T, p)$	$c_V(T, p)$	$u(T, p)$	$k_T(T, p)$	$k_S(T, p)$
$CH_3COOCH_2CH_3$	298–328	7	5.62	2.21	9.89	14.56	17.32
$CH_3COO(CH_2)_2CH_3$	298–328	7	4.53	1.19	7.12	10.11	13.08
$CH_3COO(CH_2)_3CH_3$	298–328	7	2.18	1.80	4.96	9.16	9.52
$CH_3COO(CH_2)_4CH_3$	298–328	7	0.76	0.68	3.88	6.34	7.54
$CH_3COO(CH_2)_9CH_3$	298–328	7	1.23	3.32	1.01	0.38	1.78
Average	...	...	2.86	1.84	5.37	8.11	9.85

molecules with a short alkyl chain, which is not accurately reproduced by the theory in the case of derivative properties. It should be noted that this is somewhat expected, as group contribution approaches are less suitable for the description of small molecules. As the chain length of the *n*-alkyl acetates is increased, the level of agreement between the predictions of the theory and the experimental data improves, and a very good representation is seen in the case of *n*-decyl acetate. This is also depicted in Figure 11, where the predictions of the theory for the speed of sound and the isobaric heat capacity of *n*-alkyl acetates with varying chain lengths are plotted together with the experimental data.

An assessment of the SAFT-γ Mie EoS in the prediction of the pure-component fluid-phase behavior for longer compounds not included in the parameter estimation procedure has also been performed for the *n*-alkyl acetates. The parameters for the CH_3, CH_2, and COO groups are used to predict the fluid-phase behavior of five high-molecular-weight *n*-alkyl acetates, namely *n*-nonyl, *n*-decyl, *n*-undecyl, *n*-dodecyl, and *n*-tetradecyl acetate; the deviations from the experimental data, available for the vapor pressure only, are summarized in Table VIII. From the table it can be seen that the SAFT-γ Mie approach can be extrapolated with good accuracy to the prediction of the pure component fluid-phase behavior of long-chain *n*-alkyl acetates. Aside from predictions for pure-component fluid-phase behavior the SAFT-γ Mie approach can be successfully applied to the prediction of single-phase densities and second-order thermodynamic derivative properties of long-chain esters. This is demonstrated in Figure 12, where the predictions of the theory are compared with the experimental data for the single-phase density, the speed of sound, and the isothermal and isentropic compressibility of several long-chain ethyl esters, namely, ethyl caprylate (ethyl *n*-octanoate), ethyl caprate (ethyl *n*-decanoate), ethyl laurate (ethyl *n*-dodecanoate), ethyl myristate (ethyl *n*-tetradecanoate), and ethyl palmitate (ethyl *n*-hexadecanoate), fatty acid esters of key relevance in the production of biofuels. It should be noted that these compounds are not of the same category as the ones used in the development of the COO functional group, where data for alkyl acetates were used; however, since the functional group developed is the more versatile COO group (as opposed to models where a CH_3COO group is employed) the properties of these ethyl esters can be predicted in a reliable and straightforward manner.

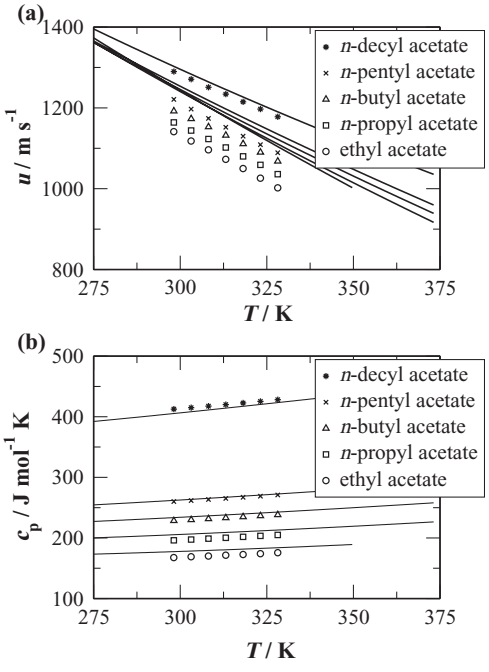

FIG. 11. Prediction of the second-order thermodynamic derivative properties of selected *n*-alkyl acetates obtained with the SAFT-γ Mie group contribution approach: (a) speed of sound u, and (b) isobaric heat capacity c_p of ethyl acetate (circles), *n*-propyl acetate (squares), *n*-butyl acetate (triangles), *n*-pentyl acetate (crosses), and *n*-decyl acetate (asterisks) at a pressure of $p = 0.1$ MPa. All symbols are experimental data[156] and the continuous curves are the predictions of the theory.

2. Binary systems

The ability to obtain information about the nature of the unlike dispersion interaction between segments belonging to the same molecule is an inherent advantageous feature of the SAFT-γ approach. For the specific case of the chemical families considered in this work, this means that the values of the unlike dispersion energies between the CH_3 and CH2 groups are obtained from pure-component data of the *n*-alkanes alone (see Table III). This allows for calculations of the fluid-phase behavior and other properties of mixtures of *n*-alkanes and/or esters in a purely predictive manner.

TABLE VIII. Percentage average absolute deviations (%AAD) for the vapor pressures $p_{vap}(T)$ and saturated liquid densities $\rho_{sat}(T)$ of the predictions with the SAFT-γ Mie group contribution approach from the experimental data (where n is the number of data points) of long-chain n-alkanes and n-alkyl acetates not included in the estimation of the group parameters. The references to the experimental data are denoted in each case.

Compound	T range [K]	n	%AAD $p_{vap}(T)$	Ref.	T range [K]	n	%AAD $\rho_{sat}(T)$	Ref.
n-$C_{15}H_{32}$	293–576	35	7.19	[157, 158]	273–633	11	0.71	[152]
n-$C_{20}H_{42}$	388–625	29	15.66	[159]	293–683	11	0.98	[152]
n-$C_{25}H_{52}$	381–461	13	29.87	[160]	293–695	11	3.10	[152]
n-$C_{30}H_{62}$	432–452	5	37.50	[160]	293–727	11	4.01	[152]
$CH_3COO(CH_2)_8CH_3$	276–309	12	1.37	[154]	…	…	…	…
$CH_3COO(CH_2)_9CH_3$	284–530	32	2.94	[154,155]	…	…	…	…
$CH_3COO(CH_2)_{10}CH_3$	288–329	14	2.31	[154]	…	…	…	…
$CH_3COO(CH_2)_{11}CH_3$	288–333	15	4.46	[154]	…	…	…	…
$CH_3COO(CH_2)_{13}CH_3$	303–340	13	2.95	[154]	…	…	…	…
Average	…	…	11.58	…	…	…	2.20	…

An example of the predictive capabilities of the SAFT-γ Mie approach is shown in Figure 13, where the theoretical description is compared to experimental data for the vapor-liquid phase behavior of the binary system n-butane+n-decane at different temperatures. It is clear that the SAFT-γ Mie predictions are in very good agreement with the experimental data for the fluid-phase equilibria of the mixture.

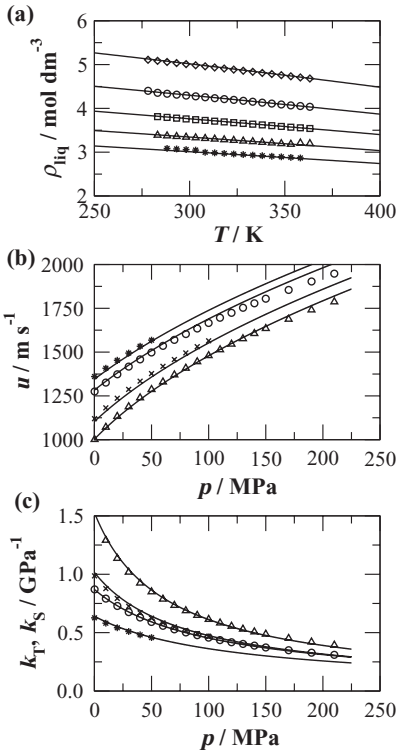

FIG. 12. Predictions of the single-phase densities and second-order thermodynamic derivative properties of long-chain ethyl esters with the SAFT-γ Mie group contribution approach: (a) single phase densities ρ_{liq} of ethyl caprylate (diamonds), ethyl caprate (circles), ethyl laurate (squares), ethyl myristate (triangles), and ethyl palmitate (asterisks) at a pressure of $p = 0.10132$ MPa;[167] (b) speed of sound u of ethyl caprate at temperatures of $T = 303.15$ K (circles) and 383.15 K and (triangles),[168] and of ethyl myristate at temperatures of $T = 293.15$ K (asterisks) and 363.15 K (crosses);[169] and (c) isothermal compressibility k_T of ethyl caprate at temperatures of $T = 303.15$ K (circles) and 383.15 K (triangles),[168] and isentropic compressibility k_S of ethyl myristate at temperatures of $T = 293.15$ K (asterisks) and 363.15 K (crosses).[169] The continuous curves are the predictions of the theory.

The improvement in the description of the near-critical fluid-phase behavior within the SAFT-γ Mie approach allows for an accurate representation of the system over a wide range of conditions, including the high-pressure critical region for isotherms at temperatures above the critical point of n-butane. The overshoot of the critical points of the phase envelopes of this binary system is significantly reduced in comparison to the results obtained with the SAFT-γ SW approach.[66]

The same parameter set can be applied to the prediction of the fluid-phase behavior of binary mixtures of compounds not included in the regression of the group parameters. An example of this is shown in Figure 14, where the predictions of the theory are compared to the experimental data for asymmetric systems of a short and an oligomeric long-chain n-alkane. More specifically, in Figure 14(a) the theoretical predictions are compared with the available experimental data for the liquid-liquid equilibria of the propane+n-hexacontane mixture at three different temperatures. This system is chosen as a prototypical example of the type of fluid-phase equilibria exhibited in polymer solutions of hydrocarbons.[135] The n-$C_{60}H_{122}$ molecule is the highest molecular-weight monodisperse n-alkane commercially available, so the mixture can be modeled without the need to account for polydispersity.[136] Polydispersity generally has to be considered in representing polymer+solvent systems and can have a significant effect on

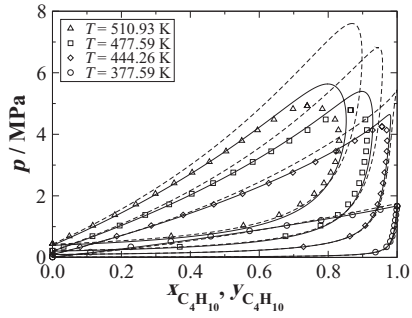

FIG. 13. Pressure-composition (p-x) isothermal slices of the fluid-phase behavior (vapor-liquid equilibria) of the n-butane + n-decane binary mixture. The continuous curves represent the predictions with the SAFT-γ Mie group contribution approach, the dashed curves the corresponding predictions with SAFT-γ SW,[66] and the symbols the experimental data at temperatures of T = 377.59 K (circles), 444.26 K (diamonds), 477.59 K (squares), and 510.93 K (triangles).[170]

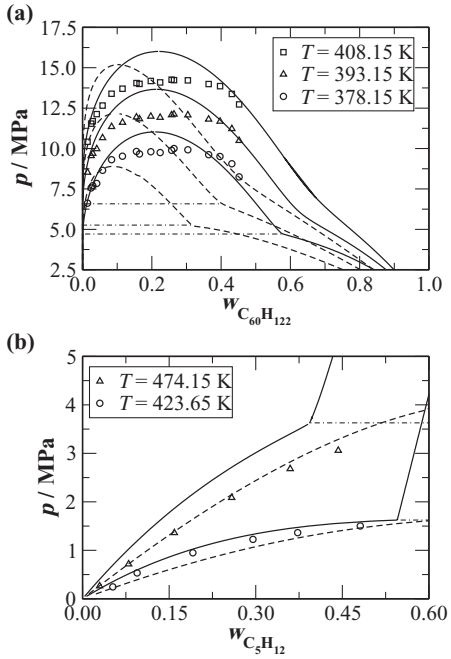

FIG. 14. Pressure-weight fraction (p-w) isothermal slices of: (a) the liquid-liquid equilibria of propane + n-hexacontane (n-$C_{60}H_{122}$); and (b) the vapor-liquid equilibria of n-pentane + low-density polyethylene (LDPE) of molecular weight 76 000 g mol^{-1}. The continuous curves represent the predictions with the SAFT-γ Mie group contribution approach, the dashed curves are the corresponding predictions with SAFT-γ SW,[66] the horizontal dashed-dotted lines are the location of three-phase equilibria, and the symbols are the experimental data[136,137] at different temperatures.

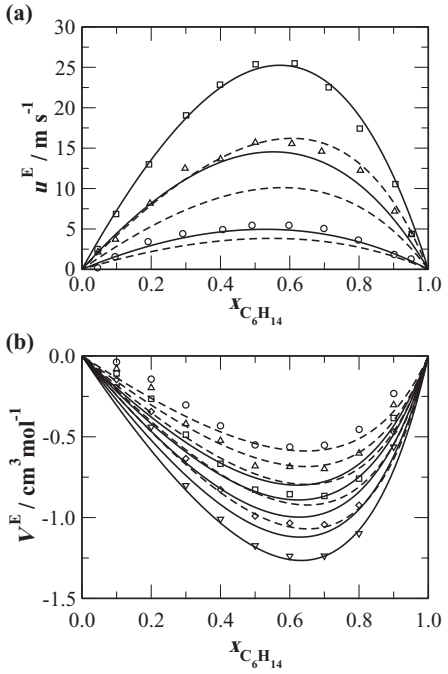

FIG. 15. Predictions of selected excess thermodynamic properties of binary mixtures of n-alkanes with the SAFT-γ Mie group contribution approach: (a) excess speed of sound u^E for n-hexane + n-dodecane (squares), n-hexane + n-decane (triangles), and n-hexane + n-octane (circles) at a temperature of T = 298.15 K;[144] and (b) excess molar volumes V^E for n-hexane + n-hexadecane at 293.15 K (circles), 303.15 K (triangles-up), 313.15 K (squares), 323.15 K (diamonds), and 333.15 K (triangles-down)[145] at a pressure of p = 0.10132 MPa. The continuous curves represent the predictions with SAFT-γ Mie group contribution approach, and the dashed curves the corresponding description with SAFT-γ SW.[66,67]

the phase boundaries, particularly in the description of liquid-liquid equilibria (e.g., see Ref. 134). From Figure 14(a) it can be seen that the SAFT-γ Mie predictions are in very good agreement with the experimentally determined phase behavior of the mixture, accurately reproducing the width of the coexistence region at higher pressures, with only a minor overshoot of the liquid-liquid critical point. The proposed methodology provides a significantly improved description of the mixture in comparison to the corresponding results obtained with the SAFT-γ SW EoS based on the SW potential.[66,67] A comparison of the predictions of the theory for the vapor-liquid equilibria of polymer-solvent systems is shown in Figure 14(b) for the mixture of n-pentane and polyethylene of molecular weight 76 000 g mol^{-1} at two temperatures. The polymer in question has quite a high degree of polydispersity characterized by a polydispersity index of 6.91;[137] this degree of polydispersity is not expected to significantly affect the vapor-liquid phase behavior of the system. From the figure it can be seen that both the SAFT-γ Mie and the SAFT-γ SW methods provide a description of similar accuracy for the vapor-liquid equilibrium of the system. As a final point it is important to emphasize that the same set of group parameters is employed for the prediction of different types of phase behavior: vapor-liquid equilibria for n-butane + n-decane and n-pentane + polyethylene, and liquid-liquid equilibria for propane + n-hexacontane.

The performance of SAFT-γ Mie can also be assessed in the prediction of excess thermodynamic properties of binary mixtures of n-alkanes. Properties such as the excess volume and enthalpy have been the subject of numerous studies,[115] including among others the seminal work of Flory and coworkers[138–140] and more recently the work of Blas and coworkers[141–143] within the SAFT framework. An example of the performance of the SAFT-γ Mie approach is illustrated in Figure 15, where the predictions of the theory are compared to experimental data for the excess speed of sound (u^E) of selected n-hexane + n-alkane binary mixtures[144] (cf. Figure 15(a)), and the excess molar volumes (V^E) of the binary mixture of n-hexane + n-hexadecane at different temperatures[145] (cf. Figure 15(b)). As for the fluid-phase behavior, the predictions of the theory are in very good agreement with the experimental data. For the excess speed of sound, the predictions of the theory are seen to be in quantitative agreement with the experimental data; the trend to lower values of the excess speed of sound as the difference in the chain lengths of the components of the mixture decreases is correctly reproduced. Quantitative agreement for the excess molar volume is seen with the data at higher temperatures, and the trend of the data to lower values with decreasing temperature is reproduced by the theory. Given the small magnitude of the data (especially at lower temperatures), and the fact that one of the components of the mixture (n-hexadecane) is not included in the parameter estimation procedure, good overall agreement of the theory with the experimental data is found. Comparing the predictions of the SAFT-γ Mie approach to the corresponding description obtained with the SAFT-γ SW

EoS, a clear improvement is seen for the excess speed of sound of the mixtures in Figure 15. In the case of the predictions of the excess volumes, both theories provide a description of equivalent accuracy, with the SAFT-γ SW in better agreement with the experimental data at the lower temperatures, and SAFT-γ Mie at the higher temperatures. Despite an accurate overall performance, it has to be noted that the theory cannot reproduce the fine features of the excess enthalpies of binary systems of asymmetric *n*-alkanes, which arise from conformational effects that the theory does not account for. Such effects can be incorporated in the general theoretical framework by including a term that treats the specific intramolecular interactions as has been shown by dos Ramos and Blas.[143]

The parameters obtained for the COO group and the unlike interaction values shown in Tables II and III allow for the prediction of properties of generic binary mixtures of *n*-alkanes and *n*-alkyl esters. A comparison between the predictions of the SAFT-γ Mie and the modified UNIFAC (Dortmund)[13] approaches for the fluid-phase behavior of selected binary mixtures is presented in Figures 16 and 17. In Figure 16, the fluid-phase behavior of mixtures of ethyl acetate with *n*-alkanes of varying chain length (*n*-pentane, *n*-octane, and *n*-decane) is presented as an isobaric temperature-composition representation. The theory accurately describes the vapor-liquid phase behavior of the mixtures studied, which are characterized by a minimum boiling azeotrope, and the shift of the azeotropic composition to higher compositions of ethyl acetate with increasing chain length of the *n*-alkane is reproduced. In Figure 17 the vapor-liquid phase behavior of a selection of mixtures of *n*-hexane with *n*-alkyl acetates of varying chain length is shown. In this case, a more distinct azeotrope is observed for *n*-hexane + ethyl acetate, the composition of which is accurately reproduced by the theory. Regarding the performance of the SAFT-γ Mie EoS in comparison to the well-established modified UNIFAC (Dortmund) GC approach, it is apparent from Figures 16 and 17 that in the case of the systems studied both approaches provide an equivalent level of agreement with the experimental data.

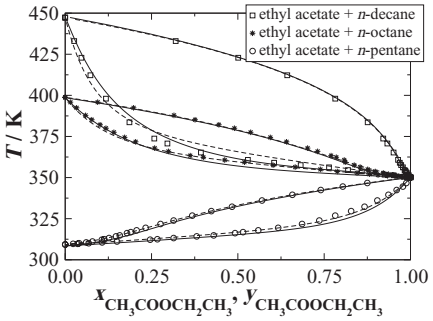

FIG. 16. Predictions of the fluid-phase behavior of binary mixtures of ethyl acetate with *n*-alkanes as temperature-composition (*T*-*x*) isobaric slices at $p = 0.10132$ MPa obtained with the SAFT-γ Mie group contribution approach. The symbols represent the experimental data[163] for the vapor-liquid equilibria of ethyl acetate + *n*-pentane (circles), ethyl acetate + *n*-octane (asterisks), and ethyl acetate + *n*-decane (squares). The continuous curves are the predictions of SAFT-γ Mie, and the dashed curves are the corresponding predictions with modified UNIFAC (Dortmund)[13] using parameters from Ref. 127.

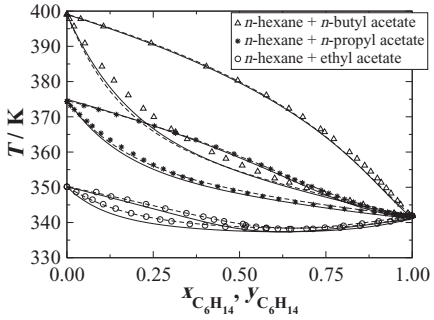

FIG. 17. Predictions of the fluid-phase behavior of binary mixtures of *n*-hexane with *n*-alkyl acetates as temperature-composition (*T*-*x*) isobaric slices at $p = 0.10132$ MPa obtained with the SAFT-γ Mie group contribution approach. The symbols represent the experimental data for the vapor-liquid equilibria of *n*-hexane + ethyl acetate (circles),[163] *n*-hexane + *n*-propyl acetate (asterisks),[163] and *n*-hexane + *n*-butyl acetate (triangles).[171] The continuous curves are the predictions of SAFT-γ Mie and the dashed curves are the corresponding predictions with modified UNIFAC (Dortmund)[13] using parameters from Ref. 127.

The adequacy of the theory in describing excess properties of mixing of binary systems of *n*-alkanes with *n*-alkyl acetates is also examined. The excess enthalpy of mixing predicted with SAFT-γ Mie for three binary mixtures of *n*-heptane with *n*-alkyl acetates of varying size (*n*-propyl, *n*-butyl, and *n*-pentyl acetate) is compared to the experimental data in Figure 18(a). It can be seen that the enthalpy of mixing of the three selected mixtures is described well, and the correct dependence of the magnitude of the excess enthalpy

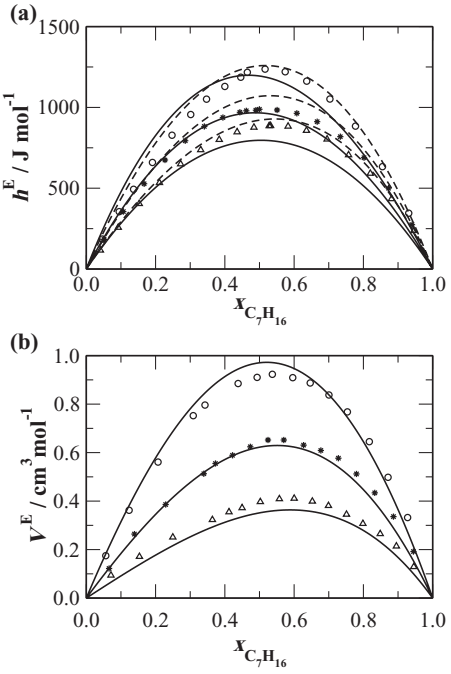

FIG. 18. Predictions for selected excess properties of binary systems of *n*-heptane with *n*-alkyl acetates obtained with the SAFT-γ Mie group contribution approach: (a) excess enthalpy h^E, and (b) excess volume V^E for *n*-heptane + *n*-propyl acetate (circles), *n*-heptane + *n*-butyl acetate (asterisks), and *n*-heptane + *n*-pentyl acetate (triangles) at a temperature of $T = 318.15$ K and a pressure of $p = 0.10132$ MPa.[172] The continuous curves represent the predictions with SAFT-γ Mie and the dashed curves (for the excess enthalpy) represent the calculations with modified UNIFAC (Dortmund)[13] using parameters from Ref. 127.

with varying chain length of the *n*-alkyl acetate is also predicted. The SAFT-γ Mie predictions are seen to be of similar accuracy to those with the modified UNIFAC (Dortmund) approach, as shown in Figure 18(a). This is very pleasing, given the small absolute values of the excess enthalpy for these mixtures ($h^E \leq 1.5$ kJ mol^{-1}). One has to bear in mind that the SAFT-γ Mie parameters are obtained predominantly from pure-component experimental data and data for selected mixtures, while the UNIFAC parameters are the result of extensive regression to binary mixture (fluid-phase behavior and other properties) data. In Figure 18(b), the predictions of the SAFT-γ Mie theory for the excess volumes of the same mixtures are compared to the experimental data. In this case, comparisons with the modified UNIFAC (Dortmund) approach are not possible, as UNIFAC is based on a lattice-fluid model and thus cannot be used directly for density calculations. The performance of the SAFT-γ Mie approach is very satisfactory, and excellent agreement between the calculations and the experimental data is seen.

Finally, we examine the performance of the theory for the prediction of second-order thermodynamic derivative properties of binary mixtures of *n*-hexane with *n*-alkyl acetates of different chain lengths. In Figure 19 a comparison of the experimental data and the SAFT-γ Mie predictions for the speed of sound (Figure 19(a)) and the excess isentropic compressibility (Figure 19(b)) is shown for binary mixtures of *n*-hexane with ethyl, *n*-pentyl, and *n*-decyl acetate. In the case of the speed of sound, and in line with the deviations reported in Table VII, it can be seen that the theory provides a qualitative description of the experimental data; the deviation in the prediction of the speed of sound in the limit of pure ethyl acetate is, however, quite significant. As the chain length of the *n*-alkyl acetate is increased, the agreement of the predictions with experiments improves, and the results for *n*-hexane + *n*-decyl acetate are seen to be in excellent agreement with the experimental data. Regarding the predictions for the excess isentropic compressibility of the same mixtures (cf. Figure 19(b)), the SAFT-γ Mie predictions reproduce the change of sign observed for mixtures of *n*-hexane with ethyl and *n*-pentyl acetate.

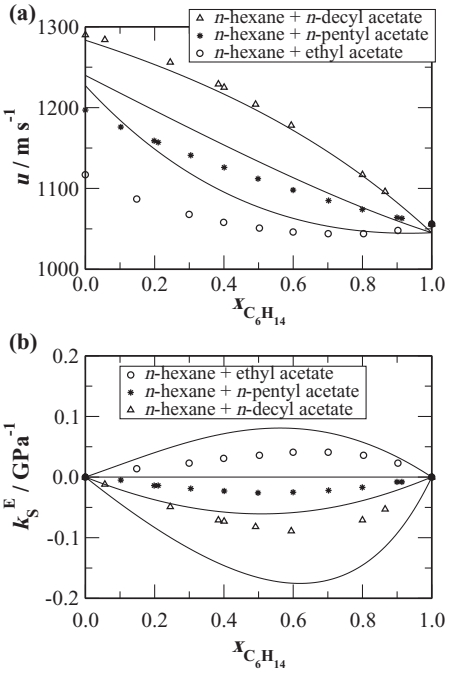

FIG. 19. Predictions of selected second-order thermodynamic derivative properties of binary mixtures of *n*-hexane with *n*-alkyl acetates obtained with the SAFT-γ Mie group contribution approach: (a) speed of sound u, and (b) excess isentropic compressibility of mixing k_S^E for *n*-hexane + ethyl acetate (circles), *n*-hexane + *n*-pentyl acetate (asterisks), and *n*-hexane + *n*-decyl acetate (triangles) at a temperature of $T = 303.15$ K and a pressure of $p = 0.10132$ MPa.[173] The continuous curves represent the predictions of the theory.

VI. CONCLUDING REMARKS

We have presented the development of the SAFT-γ Mie approach as a reformulation of the SAFT-VR Mie EoS[73] within a group contribution formalism, where the interactions between segments are represented by means of the Mie pair potential with variable attractive and repulsive exponents. The molecular model employed for the description of pure substances and mixtures is a fused heteronuclear model. Together with the implementation of the new intermolecular potential, a key novelty of the theory lies in the treatment of the monomeric segment contribution to the free energy, where a third-order perturbation expansion is employed. The performance of the theory in the description of real systems is examined in studies considering two chemical families (the *n*-alkanes and the *n*-alkyl esters), where parameters for the methyl, methylene, and carboxylate functional groups (CH_3, CH_2, and COO) are obtained from fluid-phase behavior data and single-phase densities of the pure components. In the development of the carboxylate group parameters (and the unlike parameters with the *n*-alkane groups) some data for the excess enthalpies of selected binary mixtures are used, in order to characterize better the nature of the unlike interactions.

The SAFT-γ Mie approach is shown to provide an excellent description of the pure-component properties of the correlated compounds, with average relative errors of 1.19% for the vapor pressure, 0.42% for the saturated liquid density, and 0.45% for the single-phase liquid density. It is also shown that the treatment of the monomer term proposed leads to a significant improvement in the description of the near-critical region compared to the SAFT-γ SW[66] formulation.[66] In addition to fluid-phase behavior, second-order thermodynamic derivative properties are also considered. The Mie intermolecular potential model employed in the proposed methodology allows for an accurate representation of properties such as the speed of sound, the isochoric and isobaric heat capacities, and the thermal expansion coefficient as shown in detail for the *n*-alkanes; slightly higher deviations are found for the *n*-alkyl esters.

The predictive capability of the method is examined in the description of the fluid-phase equilibria and, where available, the derivative properties of high-molecular-weight compounds not included in the estimation of the group parameters. The performance of the SAFT-γ Mie approach is found to be very satisfactory. An examination of the limit of high-molecular-weight polymers confirms the robustness of our methodology and the corresponding group

parameters obtained in this work. Finally, the performance of SAFT-γ Mie is examined in the prediction of the fluid-phase behavior and excess properties of binary mixtures of *n*-alkanes and *n*-alkanes with *n*-alkyl esters. The theory is seen to describe accurately the fluid-phase behavior of a variety of systems, for different types of phase equilibria (vapor-liquid and liquid-liquid), over a wide range of conditions, including the high-pressure critical points of the mixtures. The excess and second-order thermodynamic derivative properties of binary mixtures are also very well described. For the mixtures considered, the predictions of the fluid-phase equilibria and excess enthalpy with SAFT-γ Mie compare favorably to the calculations using the well-established modified UNIFAC (Dortmund) GC approach. The description of excess and derivative properties is a challenging task as these are known to be very sensitive to the specific molecular details, and the performance of the SAFT-γ Mie demonstrates the future potential of the theory for the study of other chemical families.

ACKNOWLEDGMENTS

V.P. is very grateful to the Engineering and Physical Sciences Research Council (EPSRC) of the UK for the award of a Ph.D. studentship. T.L. and C.A. thank the Engineering and Physical Sciences Research Council (EPSRC) of the UK for the award of postdoctoral fellowships. Additional funding to the Molecular Systems Engineering Group from the EPSRC (Grant Nos. GR/T17595, GR/N35991, EP/E016340, EP/J003840, and EP/J014958), the Joint Research Equipment Initiative (JREI) (GR/M94426), and the Royal Society-Wolfson Foundation refurbishment scheme is also gratefully acknowledged.

APPENDIX: COMPARISON BETWEEN THE SAFT-γ AND HETERO GC-SAFT-VR TREATMENT OF THE CHAIN TERM

Within a SAFT treatment the contribution due to the formation of molecular chains from monomeric segments is determined from a knowledge of the radial distribution function of the reference monomeric fluid at contact, based on Wertheim's first-order thermodynamic perturbation theory (TPT1).[47–50] Such a treatment is straightforward for homonuclear models formed from tangent segments, but, in the case of heteronuclear molecular models formed from fused segments, an alternative treatment is required since the monomeric segments forming the molecular chains may be bonded at different distances.

Different approaches have been suggested for the formulation of the chain contribution within SAFT-type theories based on fused heteronuclear molecular models. In SAFT-γ an effective TPT1 treatment is employed, where the following relation is used for the calculation of the chain term:

$$\frac{A^{\text{chain}}}{Nk_{\text{B}}T} = -\sum_{i=1}^{N_{\text{C}}} x_i \sum_{k=1}^{N_{\text{G}}} \left(\nu_{k,i}\nu_k^* S_k - 1\right) \ln g_{ii}(\bar{\sigma}_{ii}). \quad \text{(A1)}$$

The radial distribution function of the reference system of monomers at contact, $g_{ii}(\bar{\sigma}_{ii})$, is evaluated for an average molecular distance obtained as a weighted average over the sizes σ_{kl} of the constituent monomeric segments of the molecular chain.[66,67] A different formulation was proposed in the development of the hetero GC-SAFT-VR approach,[63,70] and was subsequently employed in the heterosegmented PC-SAFT approach,[71] where the Helmholtz free energy change due to chain formation is obtained based on an appropriate summation of the monomeric radial distribution function at the different intersegment contacts σ_{kl} as

$$\frac{A^{\text{chain}}}{Nk_{\text{B}}T} = -\sum_{i=1}^{N_{\text{C}}} x_i \sum_{k=1}^{N_{\text{G}}} \left[\nu_{k,i}\left(\nu_k^* S_k - 1\right) \ln g_{kk}(\sigma_{kk}) + \sum_{l=k}^{N_{\text{G}}} b_{i,kl} \ln g_{kl}(\sigma_{kl})\right], \quad \text{(A2)}$$

where $b_{i,kl}$ denotes the number of bonds between segments k and l on molecule i. It is important to note that both expressions revert to the original treatment of the chain term in the case of homonuclear chains. Equations (A1) and (A2) are written in a general form in terms of the contact value of the radial distribution function; for a given intermolecular potential the RDF can be determined from the Barker-Henderson

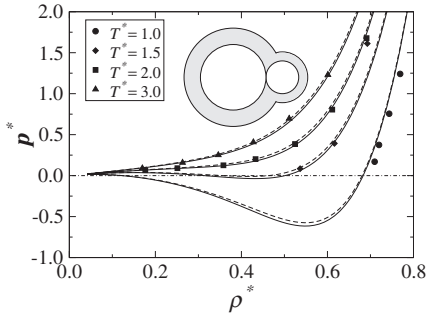

FIG. 20. Comparison of the predictions of the SAFT-γ SW and SAFT-γ^* SW approaches with isothermal-isobaric Monte Carlo simulation data for the density $\rho^* = \rho\sigma_{11}^{*3}$ dependence of the pressure $p^* = p\pi\sigma_{11}^{*3}/(6kT)$ at different temperatures $T^* = kT/\epsilon_{11}$ for tangentially bonded square-well diatomics[62] with: $\sigma_{22} = 0.5\sigma_{11}$; $\epsilon_{11} = \epsilon_{12} = \epsilon_{22}$; $\lambda_{11} = \lambda_{12} = \lambda_{22} = 1.5$. The continuous curves represent the calculations with a SAFT-γ treatment of the chain term, and the dashed curves are the results with SAFT-γ^*.

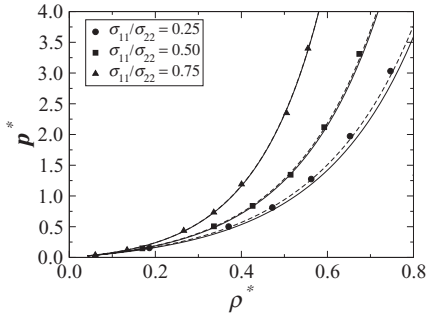

FIG. 21. Comparison of the predictions of the SAFT-γ and SAFT-γ^* approaches with Monte Carlo simulation data for the density $\rho^* = \rho\sigma_{11}^{*3}$ dependence of the pressure $p^* = p\pi\sigma_{11}^{*3}/(6kT)$ for tangentially bonded heteronuclear hard-sphere diatomics with different segment size ratios: $\sigma_{11}/\sigma_{22} = 0.25$ (circles), $\sigma_{11}/\sigma_{22} = 0.50$ (squares), and $\sigma_{11}/\sigma_{22} = 0.75$ (triangles).[54] The continuous curves represent the calculations with a SAFT-γ treatment of the chain term, and the dashed curves are the results with SAFT-γ^*.

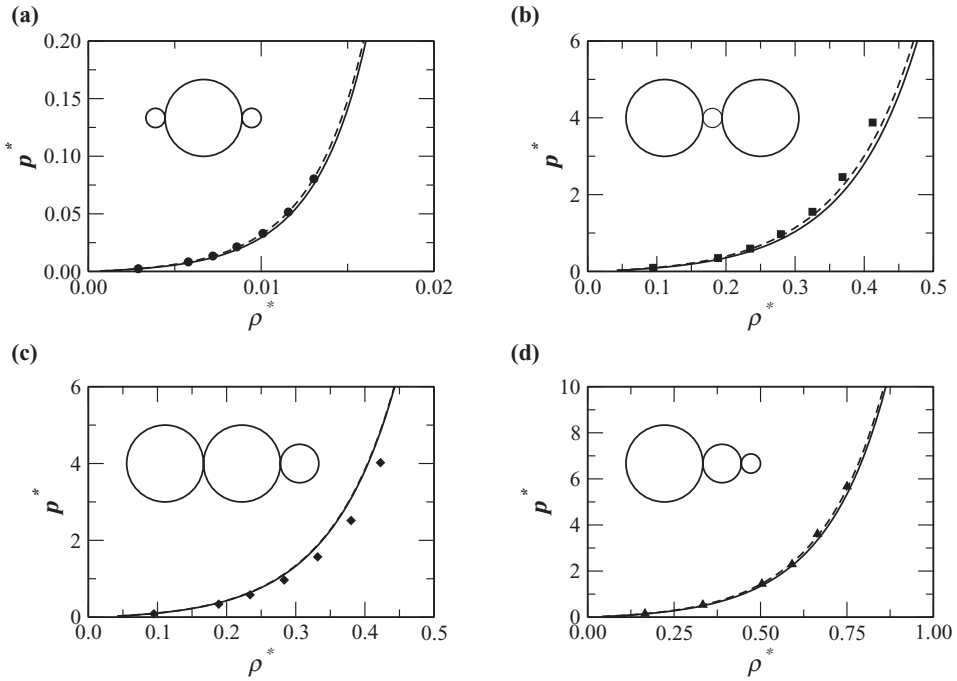

FIG. 22. Comparison of the predictions of the SAFT-γ and SAFT-γ^* approaches with Monte Carlo simulation data for the density $\rho^* = \rho\sigma_{11}^{*3}$ dependence of the pressure $p^* = p\pi\sigma_{11}^{*3}/(6kT)$ of heteronuclear hard-sphere triatomics with different segment size ratios and connectivity: (a) $\sigma_{11} = 0.25\sigma_{22} = \sigma_{33}$; (b) $\sigma_{11} = 4\sigma_{22} = \sigma_{33}$; (c) $\sigma_{11} = \sigma_{22} = 2\sigma_{33}$; and (d) $\sigma_{11} = 2\sigma_{22} = 4\sigma_{33}$.[55] The continuous curves represent the calculations with a SAFT-γ treatment of the chain term, and the dashed curves are the results with SAFT-γ^*.

perturbation theory as shown for the square-well potential in Refs. 66 and 70 and for the Mie potential in Sec. III C.

Here, we examine the performance of the two methodologies presented for the chain term based on comparison with simulation data for square-well and hard-sphere heteronuclear diatomic and triatomic molecules. Though our main interest is in models based on the Mie potential, to our knowledge there are no suitable simulation data for heteronuclear molecules formed from Mie segments. Comparisons of the theoretical treatment with simulation data for heteronuclear SW molecules should however provide a good indication of the adequacy of the approximations made in the generic chain term. A first comparison is shown in Figure 20, where calculations with the SAFT-γ[66,67] and the hetero GC-SAFT-VR[63,70] treatments of the chain term are compared to the corresponding simulation data for several pressure-density isotherms of a tangentially bonded heteronuclear square-well diatomic fluid with a fixed segment size ratio of $\sigma_{11} = 0.5\,\sigma_{22}$. It should be noted that the only difference between the SAFT-γ SW and the hetero GC-SAFT-VR calculations shown in the plot is the treatment of the chain term; the SAFT-γ theory[66,67] is used in both cases for the calculation of the monomer contribution, neglecting the minor differences between the two theories, as discussed in detail in Refs. 24 and 28. In the remainder of our current paper, this "hybrid" theory is referred to as SAFT-γ^* to distinguigh it from the original hetero GC-SAFT-VR approach. From the figure it is apparent that both approaches accurately capture the effect of the heteronuclear nature of the diatomic square-well molecule.

It is of further interest to examine how the two approaches perform for heteronuclear dimers with different segment size ratios. Simulation data for pressure-density isotherms for purely repulsive tangentially bonded heteronuclear hard-sphere dimers are compared with the theoretical description in Figure 21. The calculations are performed using the SAFT-γ and SAFT-γ^* approaches, disregarding the contributions arising from attractions between monomeric segments. From the comparison, it appears that the predictions of the two methodologies in the description of the thermodynamic properties of the heteronuclear hard-sphere dimer for similar segment sizes are almost indistinguishable. As the segments become more different in size, the SAFT-γ^* description is in better agreement with the simulation data, compared to that with the SAFT-γ calculations. However, this is of little consequence in practice as such differences in the segment size ($\sigma_{11}/\sigma_{22} \approx 0.25$) would be rather unrealistic when representing real compounds, especially considering the extension of SAFT-γ to treat large chemical groups by means of multiple identical segments.[67] The smallest segment size ratio reported in the published SAFT-γ parameter table[67] is found for between the hydroxyl OH and carbonyl C=O functional groups with a value of $\sigma_{C=O}/\sigma_{OH} \approx 0.59$.

As a final example we consider heteronuclear hard-sphere trimers. A comparison between the SAFT-γ and

TABLE IX. Group parameters for the methyl and methylene functional groups (CH_3 and CH_2) of the *n*-alkanes within the SAFT-γ^* SW approach. The optimal value of the energy of the unlike interaction is found to be $\epsilon_{CH_3-CH_2}/k_B = 240.61$ K.

Functional group k	v_k^*	S_k	λ_{kk}	σ_{kk} [Å]	ϵ_{kk}/k_B [K]
CH_3	1	0.66667	1.4335	3.8059	244.63
CH_2	1	0.33333	1.7139	3.9959	217.74

TABLE X. Percentage average absolute deviations (%AAD) for the vapor pressures $p_{vap}(T)$ and the saturated liquid densities $\rho_{sat}(T)$ of the *n*-alkanes obtained with the SAFT-γ^* SW approach from the experimental data,[161] compared to the description with the SAFT-γ SW approach.[66] *n* is the number of experimental data points for each property.

Compound	*T* range [K]	*n*	SAFT-γ SW %AAD $p_{vap}(T)$	SAFT-γ^* SW %AAD $p_{vap}(T)$	SAFT-γ SW %AAD $\rho_{sat}(T)$	SAFT-γ^* SW %AAD $\rho_{sat}(T)$
C_2H_6	91–270	38	3.93	2.89	1.02	1.89
n-C_3H_8	97–331	38	4.09	6.46	0.65	1.80
n-C_4H_{10}	139–379	38	3.44	4.81	0.55	2.06
n-C_5H_{12}	144–417	38	5.39	7.08	0.54	1.56
n-C_6H_{14}	177–455	38	3.60	4.05	0.47	1.46
n-C_7H_{16}	191–483	37	4.09	5.08	0.51	1.46
n-C_8H_{18}	216–512	38	3.69	4.68	0.45	1.47
n-C_9H_{20}	344–424	15	3.01	6.19	0.40	0.97
n-$C_{10}H_{22}$	243–553	63	4.63	5.22	0.52	1.38
Average	...	...	3.98	5.16	0.57	1.56

SAFT-γ^* calculations and the corresponding simulation data for the pressure-density isotherms of tangentially bonded heteronuclear hard-sphere trimers with different segment ratios and/or connectivity is shown in Figure 22. It should be noted that in this case, the chain contribution in SAFT-γ^* is calculated by explicitly accounting for the connectivity of the monomeric segments to form the molecular chain, while in SAFT-γ the only structural information that is taken into account is the number of occurrences of each monomeric segment. This difference in the description of the molecular chain term is not found, however, to affect the agreement of the theoretical description with the simulation data to a great extent. From this analysis it can be concluded that both approximations for the chain contribution provide a satisfactory description of the thermodynamic behavior of the heteronuclear trimers considered, with the SAFT-γ^* approach performing marginally better. The calculation of the chain contribution within SAFT-γ successfully reproduces the thermodynamic properties of heteronuclear molecules, and in that way the heteronuclear nature of the molecular model is retained within the theory at the level of the formation of the molecular chain from distinct monomers. The SAFT-γ treatment is shown to be almost indistinguishable from a SAFT-γ^* treatment, apart for extreme differences in the sizes of the segments forming the chain. However, such extreme values are of purely theoretical interest, as highly asymmetric molecular models are not usually expected to be appropriate in the modeling of real fluids. Nevertheless, it should be acknowledged that some isomers are treated differently when Eq. (A2) is used to calculate the chain contribution to the Helmholtz free-energy, whereas their properties would be the same when Eq. (A1) is used.

The comparison made thus far between SAFT-γ and SAFT-γ^* is based on simulation data for *tangentially* bonded heteronuclear models. A full comparison for *fused* segments is more difficult as an explicit relationship between the degree of overlap and the bond length has to be established. However, an assessment of the two approaches can be made by examining the description of the properties of real compounds. This is undertaken here for the chemical family of *n*-alkanes, where the description of the SAFT-γ SW approach with the parameters from Ref. 66 is compared with the corresponding results obtained using SAFT-γ^*. The SAFT-γ^* parameters for the CH_3 and CH_2 groups are obtained here using the same approach as in previous work,[66,67] with the same experimental data. Regarding the parameters, the shape factors for both the CH_3 and the CH_2 groups are assigned values of 1/3 and 2/3, respectively, while the only unlike parameter which is estimated is the energy of the unlike interaction, $\epsilon_{CH_3-CH_2}$, as opposed to the original work with hetero GC-SAFT-VR[70] where the range of the unlike interaction $\lambda_{CH_3-CH_2}$ is treated as an additional adjustable parameter. The parameters obtained with SAFT-γ^* are listed in Table IX, and the deviations for the vapor pressure and saturated liquid density are summarized in Table X. It is clear from this analysis that the SAFT-γ treatment of the chain term leads to a better description of the thermodynamic properties of real compounds compared to the description obtained within the same theory, but following the hetero GC-SAFT-VR treatment of the chain term (cf. Eq. (A2)).

[1] R. Dohrn and O. Pfohl, Fluid Phase Equilib. **194–197**, 15 (2002).
[2] W. B. Whiting, J. Chem. Eng. Data **41**, 935 (1996).
[3] S. Gupta and J. D. Olson, Ind. Eng. Chem. Res. **42**, 6359 (2003).
[4] L. E. K. Achenie, R. Gani, and V. Venkatasubramanian, *Computer Aided Molecular Design: Theory and Practice*, 1st ed. (Elsevier Science B.V., Amsterdam, The Netherlands, 2003).
[5] F. E. Pereira, E. Keskes, A. Galindo, G. Jackson, and C. S. Adjiman, "Integrated design of CO_2 capture processes from natural gas," in *Process Systems Engineering : Energy Systems Engineering*, edited by M. C. Georgiadis, E. S. Kikkinides, and E. N. Pistikopoulos (Wiley-VCH, Weinheim, 2008), Vol. 5, Chap. 8, pp. 231–248.
[6] A. Bardow, K. Steur, and J. Gross, Ind. Eng. Chem. Res. **49**, 2834 (2010).
[7] F. E. Pereira, E. Keskes, A. Galindo, G. Jackson, and C. S. Adjiman, Comput. Chem. Eng. **35**, 474 (2011).
[8] A. L. Lydersen, Engineering Experimental Station Report No. 3 (University of Wisconsin, College of Engineering, 1955).
[9] K. G. Joback and R. C. Reid, Chem. Eng. Commun. **57**, 233 (1987).
[10] L. Constantinou and R. Gani, AIChE J. **40**, 1697 (1994).
[11] J. Marrero and R. Gani, Fluid Phase Equilib. **183–184**, 183 (2001).
[12] A. Fredenslund, R. L. Jones, and J. M. Prausnitz, AIChE J. **21**, 1086 (1975).
[13] U. Weidlich and J. Gmehling, Ind. Eng. Chem. Res. **26**, 1372 (1987).
[14] A. Klamt and F. Eckert, Fluid Phase Equilib. **172**, 43 (2000).
[15] T. Holderbaum and J. Gmehling, Fluid Phase Equilib. **70**, 251 (1991).
[16] S. Skjold-Jørgensen, Fluid Phase Equilib. **16**, 317 (1984).

[17]H. P. Gros, S. Bottini, and E. A. Brignole, Fluid Phase Equilib. **116**, 537 (1996).
[18]J. Ahlers and J. Gmehling, Fluid Phase Equilib. **191**, 177 (2001).
[19]J. Ahlers and J. Gmehling, Ind. Eng. Chem. Res. **41**, 3489 (2002).
[20]J. Ahlers and J. Gmehling, Ind. Eng. Chem. Res. **41**, 5890 (2002).
[21]W. G. Chapman, K. E. Gubbins, G. Jackson, and M. Radosz, Fluid Phase Equilib. **52**, 31 (1989).
[22]W. G. Chapman, K. E. Gubbins, G. Jackson, and M. Radosz, Ind. Eng. Chem. Res. **29**, 1709 (1990).
[23]B. E. Poling, J. M. Prausnitz, and J. P. O'Connell, *The Properties of Gases and Liquids*, 5th ed. (Mc-Graw Hill, 2001).
[24]V. Papaioannou, C. S. Adjiman, G. Jackson, and A. Galindo, "Group contribution methodologies for the prediction of thermodynamic properties and phase behavior in mixtures," in *Process Systems Engineering: Molecular Systems Engineering*, edited by C. S. Adjiman and A. Galindo (Wiley-VCH, Weinheim, 2010), Chap. 4, Vol. 6, pp. 135–173.
[25]E. A. Müller and K. E. Gubbins, Ind. Eng. Chem. Res. **40**, 2193 (2001).
[26]I. G. Economou, Ind. Eng. Chem. Res. **41**, 953 (2002).
[27]S. P. Tan, H. Adidharma, and M. Radosz, Ind. Eng. Chem. Res. **47**, 8063 (2008).
[28]C. McCabe, and A. Galindo, "SAFT Associating fluids and fluid mixtures," in *Applied Thermodynamics of Fluids*, edited by A. R. H. Goodwin, J. V. Sengers, and C. J. Peters (Royal Society of Chemistry, UK, 2010), Chap. 8, pp. 215–279.
[29]M. Lora, F. Rindfleisch, and M. A. McHugh, J. Appl. Polym. Sci. **73**, 1979 (1999).
[30]J. Vijande, M. M. Piñeiro, D. Bessières, H. Saint-Guirons, and J. L. Legido, Phys. Chem. Chem. Phys. **6**, 766 (2004).
[31]S. Tamouza, J. P. Passarello, P. Tobaly, and J. C. de Hemptinne, Fluid Phase Equilib. **222–223**, 67 (2004).
[32]S. Tamouza, J. P. Passarello, P. Tobaly, and J. C. de Hemptinne, Fluid Phase Equilib. **228–229**, 409 (2005).
[33]K. E. Gubbins and C. H. Twu, Chem. Eng. Sci. **33**, 863 (1978).
[34]T. X. N. Thi, S. Tamouza, P. Tobaly, J. P. Passarello, and J. C. de Hemptinne, Fluid Phase Equilib. **238**, 254 (2005).
[35]D. Nguyen-Huynh, M. Benamira, J. P. Passarello, P. Tobaly, and J. C. de Hemptinne, Fluid Phase Equilib. **254**, 60 (2007).
[36]D. Nguyen-Huynh, J. C. de Hemptinne, R. Lugo, J. P. Passarello, and P. Tobaly, Ind. Eng. Chem. Res. **50**, 7467 (2011).
[37]J. Rozmus, J. C. de Hemptinne, and P. Mougin, Fluid Phase Equilib. **303**, 15 (2011).
[38]J. Rozmus, J. C. de Hemptinne, N. Ferrando, and P. Mougin, Fluid Phase Equilib. **329**, 78 (2012).
[39]J. Vijande, M. M. Piñeiro, J. L. Legido, and D. Bessières, Ind. Eng. Chem. Res. **49**, 9394 (2010).
[40]A. Tihic, G. M. Kontogeorgis, N. von Solms, M. L. Michelsen, and L. Constantinou, Ind. Eng. Chem. Res. **47**, 5092 (2008).
[41]A. Tihic, N. von Solms, M. L. Michelsen, G. M. Kontogeorgis, and L. Constantinou, Fluid Phase Equilib. **281**, 60 (2009).
[42]C. Le Thi, S. Tamouza, J. P. Passarello, P. Tobaly, and J. C. de Hemptinne, Ind. Eng. Chem. Res. **45**, 6803 (2006).
[43]A. J. Haslam, A. Galindo, and G. Jackson, Fluid Phase Equilib. **266**, 105 (2008).
[44]D. Nguyen-Huynh, J. P. Passarello, P. Tobaly, and J. C. de Hemptinne, Ind. Eng. Chem. Res. **47**, 8847 (2008).
[45]D. Nguyen-Huynh, T. K. S. Tran, S. Tamouza, J. P. Passarello, P. Tobaly, and J. C. de Hemptinne, Ind. Eng. Chem. Res. **47**, 8859 (2008).
[46]M. Mourah, D. Nguyen-Huyhn, J. P. Passarello, J. C. de Hemptinne, and P. Tobaly, Fluid Phase Equilib. **298**, 154 (2010).
[47]M. S. Wertheim, J. Stat. Phys. **35**, 19 (1984).
[48]M. S. Wertheim, J. Stat. Phys. **35**, 35 (1984).
[49]M. S. Wertheim, J. Stat. Phys. **42**, 459 (1986).
[50]M. S. Wertheim, J. Stat. Phys. **42**, 477 (1986).
[51]M. S. Wertheim, J. Chem. Phys. **87**, 7323 (1987).
[52]W. G. Chapman, G. Jackson, and K. E. Gubbins, Mol. Phys. **65**, 1057 (1988).
[53]G. Jackson, W. G. Chapman, and K. E. Gubbins, Mol. Phys. **65**, 1 (1988).
[54]A. L. Archer and G. Jackson, Mol. Phys. **73**, 881 (1991).
[55]M. D. Amos and G. Jackson, Mol. Phys. **74**, 191 (1991).
[56]R. P. Sear, M. D. Amos, and G. Jackson, Mol. Phys. **80**, 777 (1993).
[57]A. L. Archer, M. D. Amos, G. Jackson, and I. A. McLure, Int. J. Thermophys. **17**, 201 (1996).
[58]M. Banaszak, C. K. Chen, and M. Radosz, Macromolecules **29**, 6481 (1996).
[59]M. Banaszak and M. Radosz, Fluid Phase Equilib. **193**, 179 (2002).
[60]H. Adidharma and M. Radosz, Ind. Eng. Chem. Res. **37**, 4453 (1998).
[61]H. Adidharma and M. Radosz, Fluid Phase Equilib. **158–160**, 165 (1999).
[62]C. McCabe, A. Gil-Villegas, G. Jackson, and F. del Río, Mol. Phys. **97**, 551 (1999).
[63]Y. Peng, H. Zhao, and C. McCabe, Mol. Phys. **104**, 571 (2006).
[64]F. J. Blas and L. F. Vega, Mol. Phys. **92**, 135 (1997).
[65]J. Gross, O. Spuhl, F. Tumakaka, and G. Sadowski, Ind. Eng. Chem. Res. **42**, 1266 (2003).
[66]A. Lymperiadis, C. S. Adjiman, A. Galindo, and G. Jackson, J. Chem. Phys. **127**, 234903 (2007).
[67]A. Lymperiadis, C. S. Adjiman, G. Jackson, and A. Galindo, Fluid Phase Equilib. **274**, 85 (2008).
[68]V. Papaioannou, C. S. Adjiman, G. Jackson, and A. Galindo, Fluid Phase Equilib. **306**, 82 (2011).
[69]S. S. Ashrafmansouri and S. Raeissi, J. Supercrit. Fluids **63**, 81 (2012).
[70]Y. Peng, K. D. Goff, M. C. dos Ramos, and C. McCabe, Fluid Phase Equilib. **277**, 131 (2009).
[71]K. Paduszyński and U. Domańska, Ind. Eng. Chem. Res. **51**, 12967 (2012).
[72]T. Lafitte, D. Bessieres, M. M. Piñeiro, and J. L. Daridon, J. Chem. Phys. **124**, 024509 (2006).
[73]T. Lafitte, A. Apostolakou, C. Avendaño, A. Galindo, C. S. Adjiman, E. A. Müller, and G. Jackson, J. Chem. Phys. **139**, 154504 (2013).
[74]G. C. Maitland, M. Rigby, E. B. Smith, and W. A. Wakeham, *Intermolecular Forces: Their Origin and Determination* (Clarendon Press, Oxford, 1981).
[75]J. Gregorowicz, J. P. O'Connell, and C. J. Peters, Fluid Phase Equilib. **116**, 94 (1996).
[76]I. Polishuk, Ind. Eng. Chem. Res. **50**, 4183 (2011).
[77]X. Liang, B. Maribo-Mogensen, K. Thomsen, W. Yan, and G. M. Kontogeorgis, Ind. Eng. Chem. Res. **51**, 14903 (2012).
[78]M. R. Faradonbeh, J. Abedi, and T. G. Harding, Can. J. Chem. Eng. **91**, 101 (2013).
[79]C. M. Colina, L. F. Turrens, K. E. Gubbins, C. Olivera-Fuentes, and L. F. Vega, Ind. Eng. Chem. Res. **41**, 1069 (2002).
[80]F. J. Blas and L. F. Vega, Ind. Eng. Chem. Res. **37**, 660 (1998).
[81]F. Castro-Marcano, C. G. Olivera-Fuentes, and C. M. Colina, Ind. Eng. Chem. Res. **47**, 8894 (2008).
[82]F. Llovell and L. F. Vega, J. Phys. Chem. B **110**, 11427 (2006).
[83]F. Llovell, C. J. Peters, and L. F. Vega, Fluid Phase Equilib. **248**, 115 (2006).
[84]N. I. Diamantonis and I. G. Economou, Energy Fuels **25**, 3334 (2011).
[85]J. Chen and J.-G. Mi, Fluid Phase Equilib. **186**, 165 (2001).
[86]A. Maghari and M. S. Sadeghi, Fluid Phase Equilib. **252**, 152 (2007).
[87]A. Maghari and M. Hamzehloo, Fluid Phase Equilib. **302**, 195 (2011).
[88]F. Llovell and L. F. Vega, J. Supercrit. Fluids **41**, 204 (2007).
[89]A. M. A. Dias, F. Llovell, J. A. P. Coutinho, I. M. Marrucho, and L. F. Vega, Fluid Phase Equilib. **286**, 134 (2009).
[90]O. Vilaseca, F. Llovell, J. Yustos, R. M. Marcos, and L. F. Vega, J. Supercrit. Fluids **55**, 755 (2010).
[91]E. Forte, F. Llovell, J. P. M. Trusler, and A. Galindo, Fluid Phase Equilib. **337**, 274 (2013).
[92]M. S. Shin, Y. Lee, and H. Kim, J. Chem. Thermodyn. **40**, 688 (2008).
[93]Y. Lee, M. S. Shin, and H. Kim, J. Chem. Thermodyn. **40**, 1580 (2008).
[94]A. J. de Villiers, C. E. Schwarz, A. J. Burger, and G. M. Kontogeorgis, Fluid Phase Equilib. **338**, 1 (2013).
[95]T. Lafitte, M. M. Piñeiro, J. L. Daridon, and D. Bessières, J. Phys. Chem. B **111**, 3447 (2007).
[96]L. A. Davies, A. Gil-Villegas, and G. Jackson, Int. J. Thermophys. **19**, 675 (1998).
[97]G. Mie, Ann. Phys. (Berlin) **316**, 657 (1903).
[98]E. A. Grüneisen, Z. Elektrochem. Angew. Phys. Chem. **17**, 737 (1911).
[99]E. A. Grüneisen, Ann. Phys. (Berlin) **344**, 257 (1912).
[100]J. E. Jones, Proc. R. Soc. London, Ser. A **106**, 441 (1924).
[101]J. E. Jones, Proc. R. Soc. London, Ser. A **106**, 463 (1924).
[102]J. E. Lennard-Jones, Proc. Phys. Soc. **43**, 461 (1931).
[103]L. L. Lee, *Molecular Thermodynamics of Nonideal Fluids* (Butterworths, Boston, 1988).
[104]J. A. Barker and D. Henderson, Rev. Mod. Phys. **48**, 587 (1976).
[105]J. A. Barker and D. Henderson, J. Chem. Phys. **47**, 4714 (1967).
[106]P. Paricaud, J. Chem. Phys. **124**, 154505 (2006).
[107]T. Boublík, J. Chem. Phys. **53**, 471 (1970).

[108]G. A. Mansoori, N. F. Carnahan, K. E. Starling, and T. W. Leland, J. Chem. Phys. **54**, 1523 (1971).
[109]A. Gil-Villegas, A. Galindo, P. J. Whitehead, S. J. Mills, G. Jackson, and A. N. Burgess, J. Chem. Phys. **106**, 4168 (1997).
[110]A. Galindo, L. A. Davies, A. Gil-Villegas, and G. Jackson, Mol. Phys. **93**, 241 (1998).
[111]B.-J. Zhang, Fluid Phase Equilib. **154**, 1 (1999).
[112]N. F. Carnahan and K. E. Starling, J. Chem. Phys. **51**, 635 (1969).
[113]T. Boublík, Mol. Phys. **59**, 775 (1986).
[114]S. Dufal, T. Lafitte, A. J. Haslam, A. Galindo, and G. Jackson, "The A in SAFT: Developing the contribution of association to the free energy within a Wertheim TPT1 treatment of generic Mie fluids," Mol. Phys. (submitted).
[115]J. S. Rowlinson and F. L. Swinton, *Liquids and Liquid Mixtures*, 3rd ed. (Butterworths, 1982).
[116]K. E. Bett, J. S. Rowlinson, and G. Saville, *Thermodynamics for Chemical Engineers* (MIT Press, 1975).
[117]F. E. Pereira, G. Jackson, A. Galindo, and C. S. Adjiman, Fluid Phase Equilib. **299**, 1 (2010).
[118]PSE Ltd., gPROMS v. 3.4.0 (2011), see http://www.psenterprise.com/.
[119]S. H. Huang and M. Radosz, Ind. Eng. Chem. Res. **29**, 2284 (1990).
[120]C. McCabe and S. B. Kiselev, Ind. Eng. Chem. Res. **43**, 2839 (2004).
[121]E. Forte, F. Llovell, L. F. Vega, J. P. M. Trusler, and A. Galindo, J. Chem. Phys. **134**, 154102 (2011).
[122]F. London, Trans. Faraday Soc. **33**, 8b (1937).
[123]J. J. Potoff and D. A. Bernard-Brunel, J. Phys. Chem. B **113**, 14725 (2009).
[124]G. Jackson and K. E. Gubbins, Pure Appl. Chem. **61**, 1021 (1989).
[125]C. McCabe and G. Jackson, Phys. Chem. Chem. Phys. **1**, 2057 (1999).
[126]P. Paricaud, A. Galindo, and G. Jackson, Fluid Phase Equilib. **194–197**, 87 (2002).
[127]J. Gmehling, J. Li, and M. Schiller, Ind. Eng. Chem. Res. **32**, 178 (1993).
[128]M. Kleiner and G. Sadowski, J. Phys. Chem. C **111**, 15544 (2007).
[129]J. Gross and G. Sadowski, Ind. Eng. Chem. Res. **40**, 1244 (2001).
[130]E. W. Lemmon, M. L. Hubert, and M. O. McLinden, "NIST standard reference database 23: Reference fluid thermodynamic and transport properties - REFPROP, version 9.0," National Institute of Standards and Technology, Standard Reference Data Program, Gaithersburg (2010).
[131]C.-S. Wu and Y.-P. Chen, Fluid Phase Equilib. **100**, 103 (1994).
[132]S. J. Han, C. J. Cregg, and M. Radosz, Ind. Eng. Chem. Res. **36**, 5520 (1997).
[133]J. Gross and G. Sadowski, Ind. Eng. Chem. Res. **41**, 1084 (2002).
[134]P. Paricaud, A. Galindo, and G. Jackson, Ind. Eng. Chem. Res. **43**, 6871 (2004).
[135]A. R. Shultz and P. J. Flory, J. Am. Chem. Soc. **74**, 4760 (1952).
[136]C. E. Schwarz and I. Nieuwoudt, J. Supercrit. Fluids **27**, 145 (2003).
[137]R. K. Surana, R. P. Danner, A. B. de Haan, and N. Beckers, Fluid Phase Equilib. **139**, 361 (1997).
[138]P. J. Flory, R. A. Orwoll, and A. Vrij, J. Am. Chem. Soc. **86**, 3507 (1964).
[139]P. J. Flory, R. A. Orwoll, and A. Vrij, J. Am. Chem. Soc. **86**, 3515 (1964).
[140]R. A. Orwoll and P. J. Flory, J. Am. Chem. Soc. **89**, 6822 (1967).
[141]F. J. Blas and I. Fujihara, Mol. Phys. **100**, 2823 (2002).
[142]F. J. Blas, Mol. Phys. **100**, 2221 (2002).
[143]M. C. dos Ramos and F. J. Blas, J. Phys. Chem. B **109**, 12145 (2005).
[144]A. Touriño, M. Hervello, V. Moreno, M. Iglesias, and G. Marino, Phys. Chem. Liq. **42**, 37 (2004).
[145]M. F. Bolotnikov, Y. A. Neruchev, Y. F. Melikhov, V. N. Verveyko, and M. V. Verveyko, J. Chem. Eng. Data **50**, 1095 (2005).
[146]E. P. J. Linstrom and W. G. Mallard, *NIST Chemistry WebBook, NIST Standard Reference Database Number 69* (National Institutes of Standards and Technology WebBook, Gaithersburg MD, 20899), see http://webbook.nist.gov/ (retrieved March 2013).
[147]N. B. Vargaftik, *Handbook of Thermophysical Properties of Gases and Fluids* (Nauka, Moscow, 1972) (cited in DETHERM).
[148]E. A. Macedo and P. Rasmussen, J. Chem. Eng. Data **27**, 463 (1982).
[149]R. L. Gardas, I. Johnson, D. M. D. Vaz, I. M. A. Fonseca, and A. G. M. Ferreira, J. Chem. Eng. Data **52**, 737 (2007).
[150]S. Young and G. L. Thomas, J. Chem. Soc., Trans. **63**, 1191 (1893).
[151]E. Lladosa, J. B. Montón, M. C. Burguet, and R. Muñoz, J. Chem. Eng. Data **53**, 108 (2008).
[152]G. Liessmann, W. Schmidt, and S. Reiffarth, Data Compilation of the Saechsische Olefinwerke Boehlen, Germany (1995) (cited in DETHERM).
[153]W. V. Steele, R. D. Chirico, S. E. Knipmeyer, and A. Nguyen, J. Chem. Eng. Data **41**, 1255 (1996).
[154]E. L. Krasnykh, S. P. Verevkin, B. Koutek, and J. Doubsky, J. Chem. Thermodyn. **38**, 717 (2006).
[155]E. F. Meyer, M. J. Awe, and R. E. Wagner, J. Chem. Eng. Data **25**, 371 (1980).
[156]S. L. Oswal, P. Oswal, P. S. Modi, J. P. Dave, and R. L. Gardas, Thermochim. Acta **410**, 1 (2004).
[157]S. Salerno, M. Cascella, D. May, P. Watson, and D. Tassios, Fluid Phase Equilib. **27**, 15 (1986).
[158]C. Viton, M. Chavret, E. Behar, and J. Jose, Int. Electron. J. Phys. Chem. Data **2**, 215 (1996) (cited in DETHERM).
[159]R. D. Chirico, A. Nguyen, W. V. Steele, M. M. Strube, and C. Tsonopoulos, J. Chem. Eng. Data **34**, 149 (1989).
[160]T. Sawaya, I. Mokbel, N. Ainous, E. Rauzy, C. Berro, and J. Jose, J. Chem. Eng. Data **51**, 854 (2006).
[161]B. D. Smith and R. Srivastava, *Thermodynamic Data for Pure Compounds Part A: Hydrocarbons and Ketones* (Elsevier, Amsterdam, 1986).
[162]L. Pias, M. I. Paz-Andrade, F. Sarmiento, E. Rodriguez-Nuñez, and J. Fernandez, Fluid phase Equilib. **28**, 183 (1986).
[163]L. Fernández, E. Pérez, J. Ortega, J. Canosa, and J. Wisniak, J. Chem. Eng. Data **55**, 5519 (2010).
[164]J.-L. Daridon, H. Carrier, and B. Lagourette, Int. J. Thermophys. **23**, 697 (2002).
[165]S. Dutour, J.-L. Daridon, and B. Lagourette, High Temp.-High Press. **33**, 371 (2001).
[166]P. Zoller and D. J. Walsh, *Standard Pressure-Volume-Temperature Data for Polymers* (Technomic, Lancaster-Basel, 1995).
[167]M. J. Pratas, S. Freitas, M. B. Oliveira, S. C. Monteiro, A. S. Lima, and J. A. P. Coutinho, J. Chem. Eng. Data **55**, 3983 (2010).
[168]E. H. I. Ndiaye, D. Nasri, and J. L. Daridon, J. Chem. Eng. Data **57**, 2667 (2012).
[169]E. H. I. Ndiaye, M. Habrioux, J. A. P. Coutinho, M. L. L. Paredes, and J. L. Daridon, J. Chem. Eng. Data **58**, 1371 (2013).
[170]H. H. Reamer and B. H. Sage, J. Chem. Eng. Data **9**, 24 (1964).
[171]L.-C. Feng, C.-H. Chou, M. Tang, and Y.-P. Chen, J. Chem. Eng. Data **43**, 658 (1998).
[172]J. Ortega, F. Espiau, and F. J. Toledo, J. Chem. Thermodyn. **36**, 193 (2004).
[173]S. L. Oswal, P. Oswal, and J. P. Dave, J. Mol. Liq. **94**, 203 (2001).